Acta Geologica Polonica, Vol. 74 (2024), No. 3, e21
DOI: 10.24425/agp.2024.151751

Neogene–Quaternary paleoenvironments and kerogen assessment of the NDO B-1 well, offshore Nile Delta, Egypt, Eastern Mediterranean: palynological evidence

MAGDY S. MAHMOUD*, AMR S. DEAF and MENNAT-ALLAH T. EL HUSSIENY

Department of Geology, Faculty of Science, Assiut University, Assiut 71516, Egypt;
** Corresponding author: magdysm@aun.edu.eg; magdysm@yahoo.com*

ABSTRACT:

Mahmoud, M.S., Deaf, A.S. and El Hussieny, M.-A.T. 2024. Neogene–Quaternary paleoenvironments and kerogen assessment of the NDO B-1 well, offshore Nile Delta, Egypt, Eastern Mediterranean: palynological evidence. *Acta Geologica Polonica*, **74** (3), e21.

Palynofacies and palynological investigations conducted on the Neogene–Quaternary succession from the NDO B-1 well, located in the offshore Nile Delta, Egypt, in the Eastern Mediterranean, suggest generally shallow marine (neritic) conditions. These environments are manifested by the overall palynofacies composition and the occurrence of dinoflagellate cysts (e.g., *Spiniferites* spp., *Lingulodinium* spp., *Hystrichokolpoma* spp., *Homotryblium* spp. and *Selenopemphix* spp.). Neritic environments are suggested for the lower and middle Miocene Sidi Salim, and the Pliocene to Pleistocene upper Kafr El Sheikh, El Wastani and Mit Ghamr formations, while shallower, coastal to inner neritic settings were interpreted for the late Miocene (Qawasim and Rosetta formations) and early Pliocene (Abu Madi and lower Kafr El Sheikh formations). Anoxic conditions existed during the deposition of the studied well succession, which can be seen from the occurrence of imprints of pyrite crystals and some types of oxygen-sensitive dinoflagellate cysts. The palynofacies fluctuated repeatedly between Amorphous Organic Matter (AOM)-dominated and phytoclast-dominated intervals, of kerogen types II and III, respectively. The spore coloration index (SCI) of indigenous thin-walled palynomorphs confirms thermally mature sediments, generative of dry gas and wet gas/condensates. Reworking during the deposition of the upper Sidi Salim, Qawasim and Rosetta formations is inferred from the occurrence of Cretaceous dinoflagellate cysts and pollen.

Key words: Palynofacies; Palynomorphs; Kerogen; Offshore Egypt.

INTRODUCTION

The Nile Delta covers an area of about 22,000 km^2 and is one of the best-known deltas in the world. It contains a thick sedimentary succession covering the basement rocks and is considered a portion of the Eastern Mediterranean Basin, i.e., the last remnants of Neotethys (see Aksu *et al.* 2005 and references therein). The Nile Delta has recently become an important petroleum (gas and condensate) producing province in Egypt, mainly from reservoirs located in Miocene and Pliocene rocks. The Abu Madi, Qawasim and Kafr El Sheikh formations contain the major hydrocarbon producing rock units in the area (e.g., El Nady and Harb 2010; Nabawy *et al.* 2023). Extensive palynological research conducted in the Nile Delta area has been focused mainly on the biostratigraphy, paleoecology and source-rock evaluation of the Neogene subsurface deposits in the region. Due to age constraints, the siliciclastics across the Messinian/Zanclean transition were assigned to different rock units (i.e., Qawasim and Abu

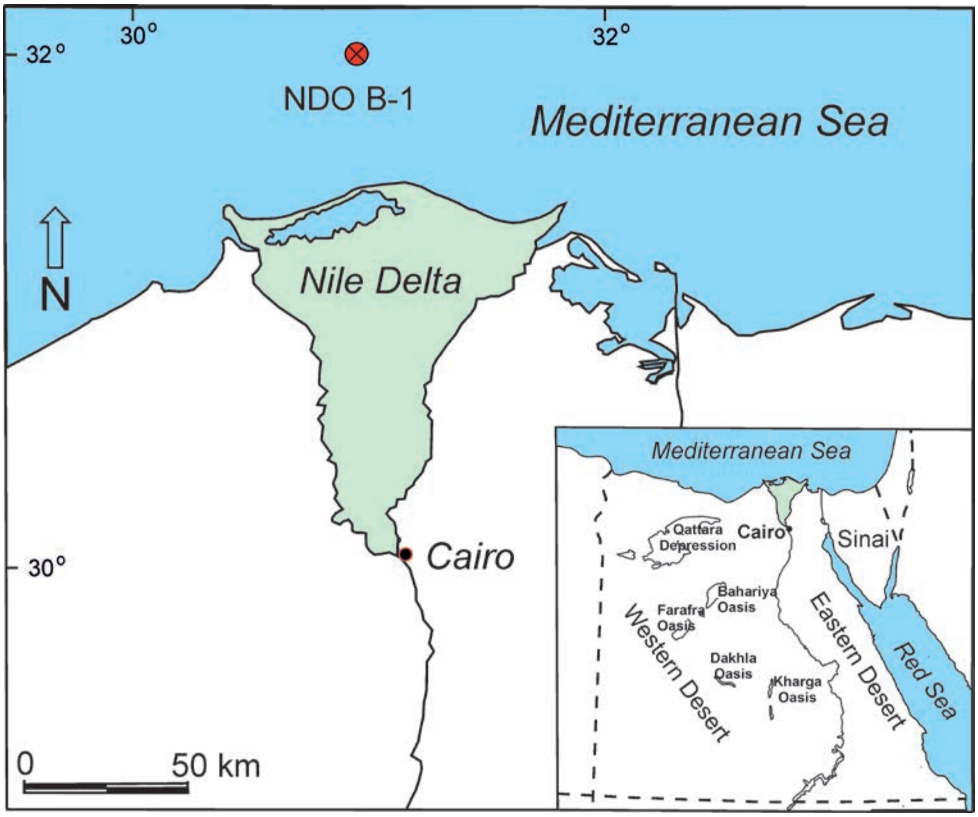

Text-fig. 1. Geographic map showing the location of the NDO B-1 well, offshore Nile Delta, Egypt.

Madi formations, see Rizzini *et al.* 1978 and E.G.P.C. 1994). The Abu Madi Fm. was recently described as bounded at the base and top by erosional and drowning unconformities, respectively. It was interpreted to record the progressive drowning of an incised valley, created by a sea-level drop in the late Messinian (Metwalli *et al.* 2023).

Recently, palynofacies investigations in Egypt were integrated with other palynological studies (e.g., El Diasty *et al.* 2019; Deaf *et al.* 2020; El Atfy 2021; Mahmoud and Khalaf 2023; Saleh *et al.* 2024). As a result, insights into the sedimentary (paleo)environments and source rock potential of the palynological organic matter (POM) have been made on an easier and cheaper basis. The present work focuses on the paleoenvironmental reconstruction of the Neogene–Quaternary sediments, penetrated by the NDO B-1 well located in the offshore Nile Delta (Text-fig. 1), carried out by investigating the total palynofacies categories. Palynomorphs, such as pollen, spores, freshwater algae and dinoflagellate cysts played an important role in this context. Emphasis was placed on the environmental significance of the total palynofacies in recognizing paleoenvironments and redox conditions of the host sediments. The work was also extended to evaluate the potential of the investigated rock units as hydrocarbon sources. This was achieved by studying the colors of thin-walled palynomorphs to infer their degree of thermal maturity, by applying the spore coloration index (SCI) on a visual basis (e.g., Pearson 1984; Traverse 2007). The established color ranges were also used to confirm reworking from older rock units.

GEOLOGICAL SETTING

Shallow marine Jurassic carbonates are the oldest rocks in the Nile Delta Basin; they are overlain by Lower Cretaceous strata. During the Late Cretaceous, the Nile Delta area was part of the Tethys Ocean. Thin Upper Cretaceous to Eocene rocks are recorded due to the impact of the Syrian Arc folding. Thermal subsidence during the Paleogene contributed to the accumulation of clastic successions in the Nile Delta (e.g., Leila *et al.* 2023). Tectonics in the Nile Delta played a crucial role in the formation of many paleo-highs and lows, which influenced the facies distribution. Continuous subsidence along the hinge zone caused thickening of the Neogene sediments in the North Nile Delta Basin (Sestini 1995). The deltaic sequence of the Nile Delta consists of two clastic successions, separated by an unconformity surface related to the Messinian Salinity Crisis (MSC) event, as mentioned in Shalaby and Sarhan (2023). The pre-Messinian sediments exhibit throughout evidence of contraction deformation (e.g., Hamouda and El-Gharabawy 2019), while the post-Messinian strata reflect a typical deltaic environment (e.g., Sarhan *et al.* 2014). However, the paleoenvironmental interpretation, based mainly on paleontological and sedimentological data, of the Neogene–Quaternary succession in the Nile Delta area remains controversial. Based on well data (stratigraphy, sedimentology, paleontology and seismic record), Rizzini *et al.* (1978) suggested an outer shelf deep marine environment for the Sidi Salim Fm. (Neogene–Quaternary). This was confirmed recently in onshore areas by planktonic foraminifera and calcareous nannoplankton (El-Kahawy *et al.* 2022). The Qawasim and Rosetta formations were interpreted as deposited under restricted (lagoonal) (El-Kahawy *et al.* 2022), fluvio-deltaic (Rizzini *et al.* 1978) or prodelta/delta front (Leila *et al.* 2019) environments. Rizzini *et al.* (1978) stated that a Lower Pliocene sandy formation (i.e., Abu Madi Fm.) lies on a fairly pronounced erosional surface, which followed the accumulation of the Qawasim and Rosetta formations. The environment of the Abu Madi Fm. was interpreted as littoral to outer neritic (Shebl *et al.* 2019), continental to marginal marine (estuarine) (Leila *et al.* 2019) or restricted marine (lagoonal) (El-Kahawy *et al.* 2022). The Kafr El Sheikh Fm. represents a return to an open marine, middle/outer neritic to upper bathyal setting (Rizzini *et al.* 1978; Zaghloul *et al.* 2001; El-Kahawy *et al.* 2022). Saleh *et al.* (2024) proposed an alternative paleoenvironmental interpretation for this rock unit based on data from the NDO B-1 well (see Table 1). They stated that the hydrocarbon source-rock potential of the Neogene deposits in the Nile Delta area requires more emphasis on the degree of dilution of the organic matter by the Nile River influx.

LITHOSTRATIGRAPHY

The Neogene–Quaternary rock succession in the NDO B-1 well is subdivided according to information presented in N.C.G.S. (1976), Rizzini *et al.* (1978), E.G.P.C. (1994) and Makled *et al.* (2017) (Text-figs 2 and 3). The relatively uniform Neogene–Quaternary succession of the Nile Delta starts with pelitic (Middle–Upper Miocene) deposits representing a deep sea or outer neritic environment (Sidi Salim Fm.), which terminates abruptly in the Messinian with the deposition of a fluvio-deltaic series (Qawasim Fm.) and evaporites (Rosetta Fm.). A Lower Pliocene sandy basal rock unit (Abu Madi Fm.) lies on an erosional surface, followed by a shale unit representing open-sea type sediments (Kafr El Sheikh Fm.). Independent dating of these rock units in the NDO B-1 well, based on planktonic foraminifera (Ouda and Obaidala 1995; Makled *et al.* 2017) and calcareous nannoplankton (Mandur and Makled 2016) is available.

The Sidi Salim Fm. (Middle–Upper Miocene; Langhian to Tortonian) is composed of clays with few intervals of dolomitic marls, sandstone and siltstone interbeds (about 448 m thick in its type section, Sidi Salim-1 well). The base is not recognizable in the center of the delta and the formation top is traced below the thick sandy and conglomeratic beds of the overlying Qawasim Fm.

The Qawasim Fm. (Upper Miocene; Messinian) consists of sand pebbles, sandstones and conglomerates with a sandy matrix interbedded with clay layers. The type section of this unit is in the Qawasim-1 well (932 m thick). These thick sandy and conglomeratic beds have a lenticular shape and exhibit slump structures. Fauna is scarce but the sandstones are rich in plant remains.

The Rosetta Fm. (Upper Miocene; Messinian) (~ 39 m thick) is composed of anhydrite layers interbedded with thin clay beds, which are barren of fossils. In the southern parts of the Nile Delta area the formation is missing. In the north, the formation ends at the levels where Lower Pliocene marine clays appear.

The Abu Madi Fm. (Lower Pliocene; Zanclean) consists of thick layers (321 m in the type section) of sand and clay interbeds. Conglomerates are more frequent in the basal parts of the formation. Foraminifera are frequent in the clay intervals and are typical of the Lower Pliocene of the Mediterranean Sea (Cita 1973). The base of the formation lacks fauna and the lower sands show large-scale cross-bedding, with bioturbation frequent in the clays.

The Kafr El Sheikh Fm. (Pliocene; Zanclean to Piacenzian) consists of clay and sand interbeds, up to 1457 m thick and extends laterally over the whole delta area. Its top is easily recognizable from the overlying El Wastani Fm. The great sand influx causes the accumulation of littoral fauna, with *Ammonia* spp. and *Elphidium* spp. The formation was accumulated in a neritic to basinal setting.

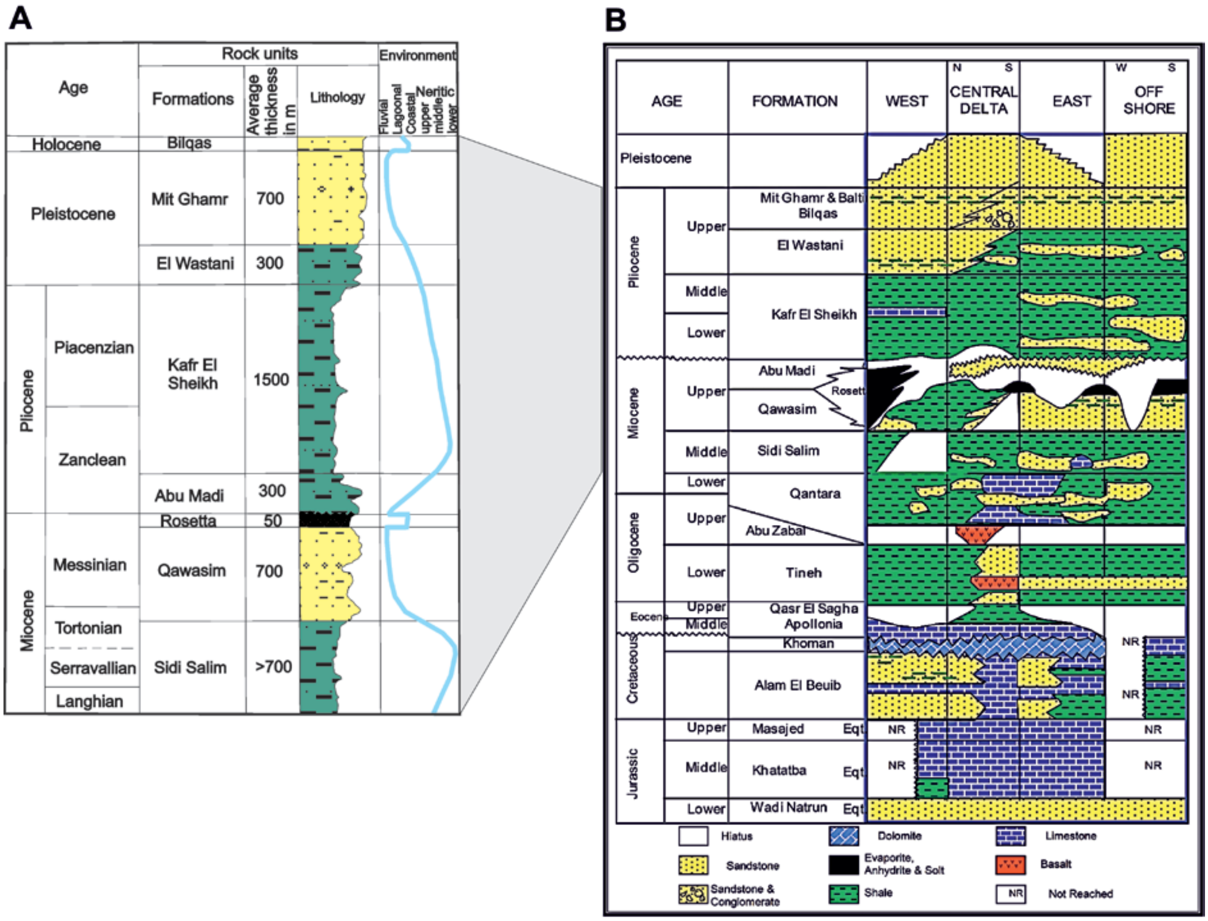

Text-fig. 2. Stratigraphy of the Nile Delta area. A – Neogene–Quaternary stratigraphic column, indicating average thicknesses and environmental trends of the examined formations (after Rizzini *et al.* 1978). B – Generalized lithostratigraphic column of the Jurassic–Quaternary interval (after E.G.P.C. 1994).

The El Wastani Fm. (Lower Pleistocene; Gelasian) is made up of 122 m thick sands interbedded with thin clays, soft and sandy, which become thinner toward the top of the formation. This unit is transitional between the shelf facies of the underlying Kafr El Sheikh Fm. and the coastal/continental sands of the overlying Mit Ghamr Fm. It shows large progradational foresets and may also contain deltaic deposits.

The Mit Ghamr Fm. (Lower Pleistocene; Gelasian to Calabrian), consists of 462 m interbedded sands and clays in the type section. The sands are quartzose, medium to coarse-grained. The pebbles consist of quartzite, chert and dolomite. Some peat horizons also occur. The formation represents a filling of the basin by coastal sands or deposits from Nile flooding. The formation represents the terminal unit of the Pliocene/Pleistocene cycle within the Nile Delta.

MATERIAL AND METHODS

This work deals with the Neogene–Quaternary succession of the NDO B-1 well, drilled at the intersection of 32º05′57″ N and 30º53′16″ E, located in the offshore Nile Delta (eastern Mediterranean), Egypt, drilled by ESSO in 1975. Fifty-three ditch samples (Text-fig. 3) were digested by HCl (35%) and HF (40%) following the standard palynological processing techniques (e.g., Traverse 2007) to remove carbonates and silicates, respectively. Residues were sieved through a 15 µm mesh. Oxidizing agents and/or excessive ultrasonic treatments were avoided during the original preparation. Part of the digested residue was treated by ultrasonic vibration for a few seconds to eliminate AOM and concentrate the palynomorphs. Permanent slides were prepared using glycerin jelly as a mounting medium for light micros-

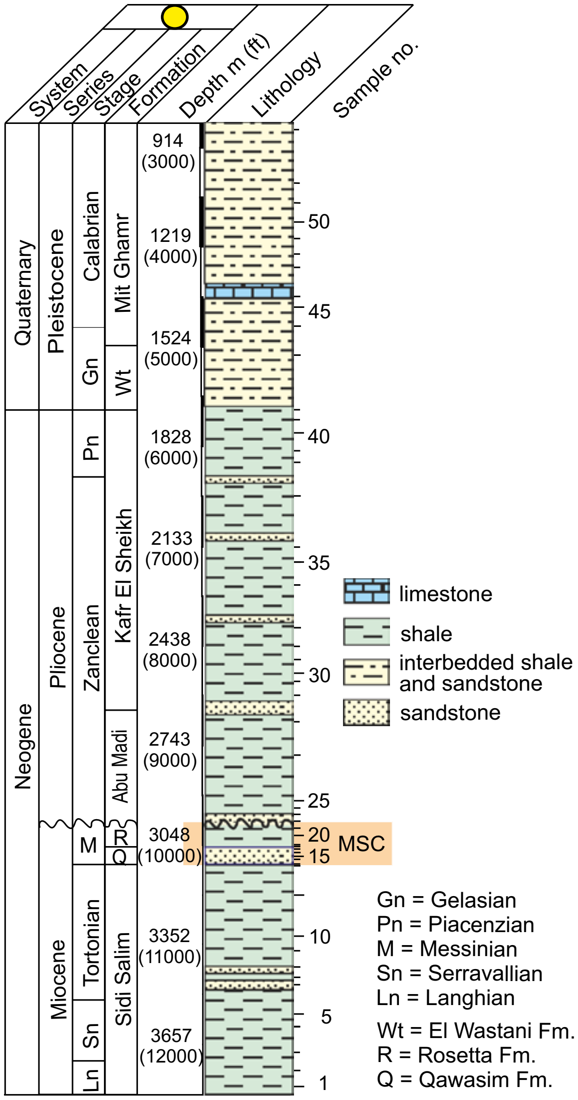

Text-fig. 3. Chrono- and lithostratigraphy of the Neogene–Quaternary succession of the investigated NDO B-1 well and location of the studied samples. Original composite log by E.S.S.O. (1975); chronostratigraphy (marked with a yellow dot) after Makled and Mandur (2016) and Mandur and Makled (2016) for calcareous nannoplankton, and Makled *et al.* (2017) for planktonic foraminifera. MSC marks the Messinian Salinity Crisis interval.

copy. Slides were examined using a Leica DM LB2 light microscope equipped with a Leica DFC 280 digital camera at the Department of Geology, Assiut University (Egypt). Examples of dinoflagellate cysts, pollen grains and other palynological matter are shown in Text-figs 4–6.

Two datasets were prepared in order to express the relative abundances of the palynofacies categories (500 particles per sample) and palynomorphs (at least 200 palynomorphs per sample), except of samples nos. 5 and 15 where palynomorphs were sparce. Usually, three to four slides from each productive sample were prepared to account for palynomorphs and palynodebris. The palynological marine index (PMI) (Helenes *et al.* 1998) was calculated from the total recovered palynomorph content, using the formula PMI = (Rm/Rt + 1) 100, where Rm refers to the species richness of marine palynomorphs (dinoflagellate cysts and microforaminiferal linings) and Rt refers to the richness of terrestrial palynomorphs (pollen, spores and freshwater algae). The marine/continental (M/C) ratio was calculated as the number of marine categories (dinoflagellate cysts + microforaminiferal linings) divided by the sum of total palynomorphs ×100. We also calculated the ratio of sensitive dinoflagellate cysts by dividing the number of sensitive cysts by the total number of dinoflagellate cysts ×100. The sensitivity of present-day representatives in modern seas to excess oxygen during their accumulation in bottom sediments was documented by Zonneveld *et al.* (2007). Moreover, the *Pediastrum*/marine ratio was calculated as the number of *Pediastrum* spp. divided by the sum of *Pediastrum* spp. and dinoflagellate cysts + microforaminiferal linings (modified after Adeonipekun *et al.* 2023, excluding *Botryococcus* spp. which is absent here). Palynomorph and palynofacies data were presented on a set of ternary diagrams to infer the paleoenvironmental conditions of palynomorphs (Federova 1977; Duringer and Doubinger 1985; Traverse 1988), palynofacies (Tyson 1993, 1995), kerogen types (Cornford 1979) and hydrocarbon potential (Dow 1982), along with other graphic presentations. The colors of thin-walled palynomorphs were applied to infer the degree of thermal maturity and reworking of the investigated sediments using the standard color chart adapted after Pearson (1984) and Traverse (2007).

RESULTS

Palynofacies

The palynofacies categories fluctuate throughout the studied succession and were dominated by phytoclasts and AOM (see Text-figs 6 and 7; Appendix 1). Phytoclasts were the main constituents of the palynofacies, more than 50% of the total kerogen in most of the succession. Their acme was seen in samples nos. 8 (80.4%, Sidi Salim Fm.), 14 (82.5%, Qawasim Fm.), 27 (87.1%, Abu Madi Fm.), 32 (84.3%, Kafr El Sheikh

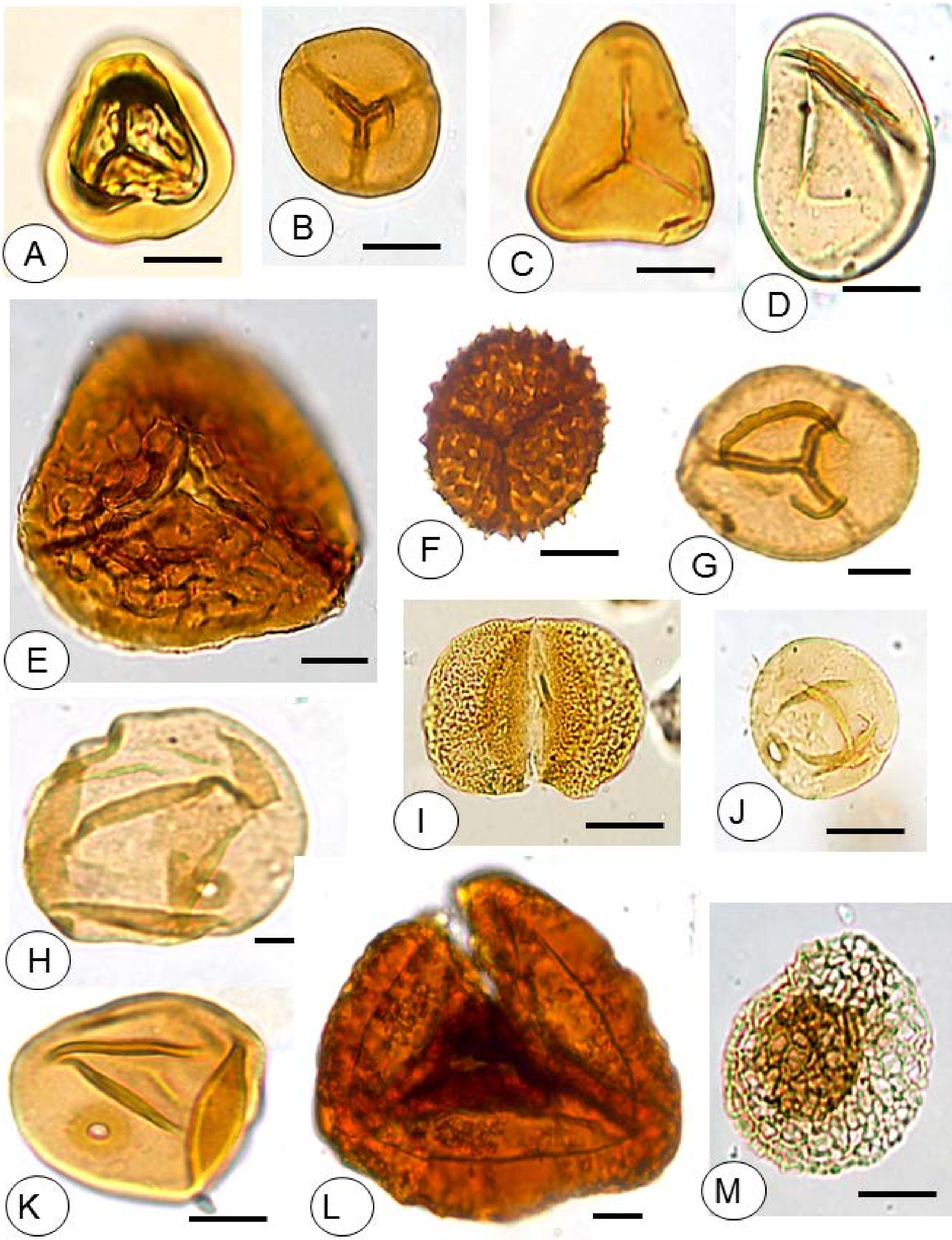

Text-fig. 4. Terrestrial palynomorphs of the NDO B-1 well. A – *Polypodiacoisporites simplex* Sah, 1967 *sensu* Eisawi and Schrank, 2008; 53h, 856 m, 29.7/107.6; B, G – cf. *Annulispora* sp.; B – 36b, 2133 m, 37/111.1; G – 16b, 3078 m, 41.4/109.7; C – *Deltoidospora* sp.; 28b, 2590 m, 34.1/99.2; D – *Laevigatosporites* sp. (monolete spore); 48c, 1249 m, 46/110; E – *Lycopodiumsporites* sp.; 22b, 2987 m, 36.1/106.3; F – Ornamented (echinate-verrucate) spore, 51a, 1075 m, 38.4/107.5; H, J – Poaceae (Gramineae); H – 30d, 2499 m, 41.3/109; J – 25b, 2919 m, 46.6/100.2; I – Bisaccate pollen; 1k, 3797 m, 34.6/99.6; K – Poaceae [*Graminidites annulatus* (Van der Hammen) Potonié, 1960]; 30b, 2499 m, 48.4/100; L – ?*Murospora* sp. (?reworked); 9c, 3340 m, 25/105.9; M – *Afropollis jardinus* (Brenner) Doyle, Jardiné and Doerenkamp, 1982 (reworked); 20k, 3041 m, 44.8/110.9. Slide numbers (equivalent to sample numbers), depths (in meters) and microscope co-ordinates are given for every illustrated specimen. Scale bar = 20 µm.

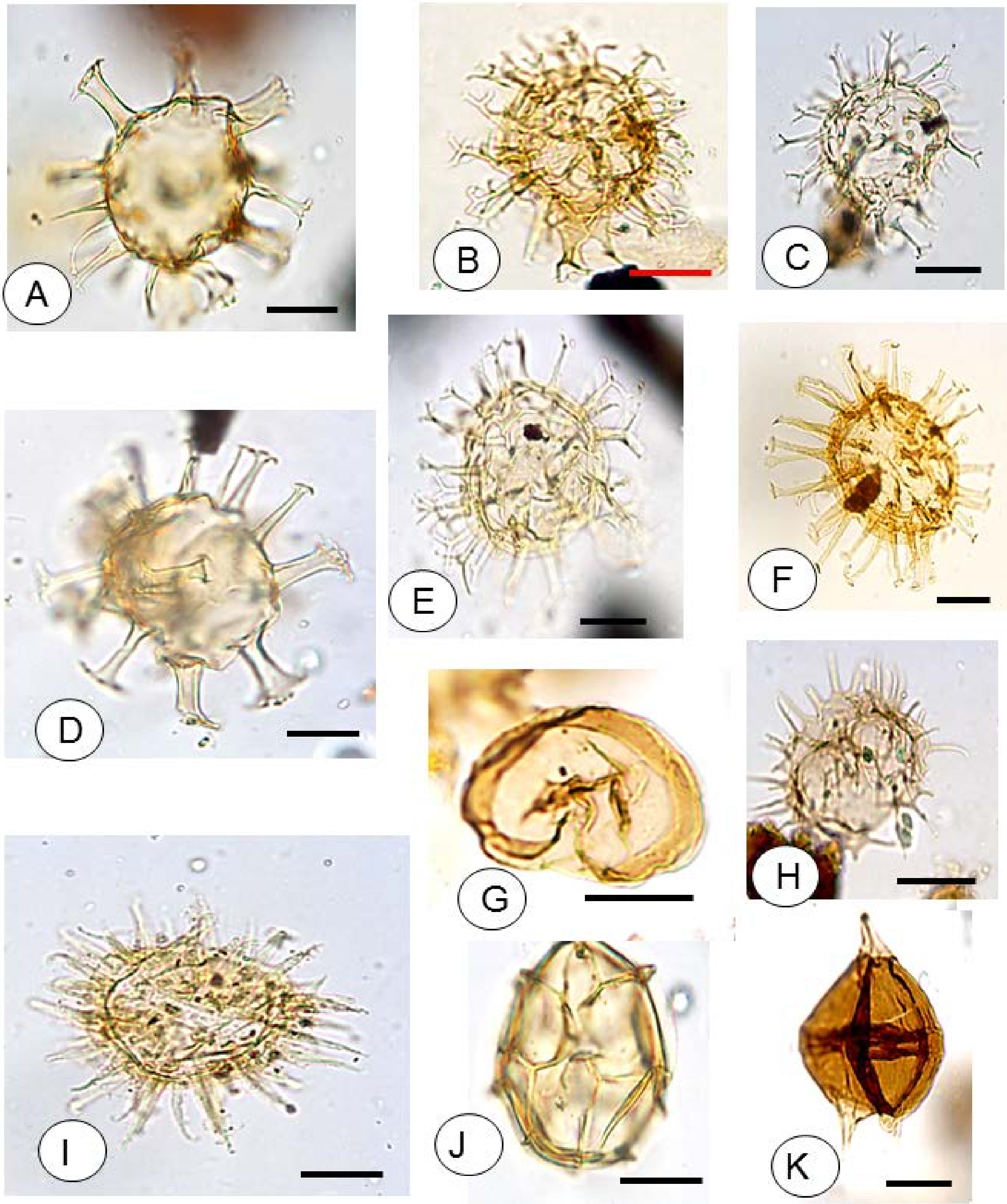

Text-fig. 5. Dinoflagellate cysts of the NDO B-1 well. A – *Hystrichokolpoma* sp.; 51a, 1075 m, 50.5/101.5; B – *Spiniferites* sp.; 2g, 3779 m, 44.2/109.3; C, E – Spiniferate cysts (*Spiniferites/Achomosphaera* Group); C – 49d, 1194 m, 52.7/104.9, E – 39d, 1859 m, 39.1/101; D – cf. *Hystrichokolpoma* sp.; 51c, 1075 m, 33.2/102.4; F – cf. *Polysphareridium zoharyi* (Rossignol) Bujak, Downie, Eaton and Williams, 1980; 2i, 3779 m, 48.2/106.9; G – *Selenopemphix nephroides* (Benedek) Benedek and Sarjeant, 1981; 4d, 3572 m, 39/101; H – *Selenopemphix quanta* (Bradford) Matsuoka, 1985; 14c, 3090 m, 44.6/110.1; I – *Lingulodinium machaerophorum* (Deflandre and Cookson) Wall, 1967; 40a, 1792 m, 36/114.8; J – *Impagidinium patulum* (Wall) Stover and Evitt, 1978; 48a, 1249 m, 38.3/104.4; K – *Cerodinium granulostriatum* (Jain and Millepied) Lentin and Williams, 1987 (reworked); 9d, 3340 m, 48.1/96. Slide numbers (equivalent to sample numbers), depths (in meters) and microscope co-ordinates are given for every illustrated specimen. Scale bar = 20 µm.

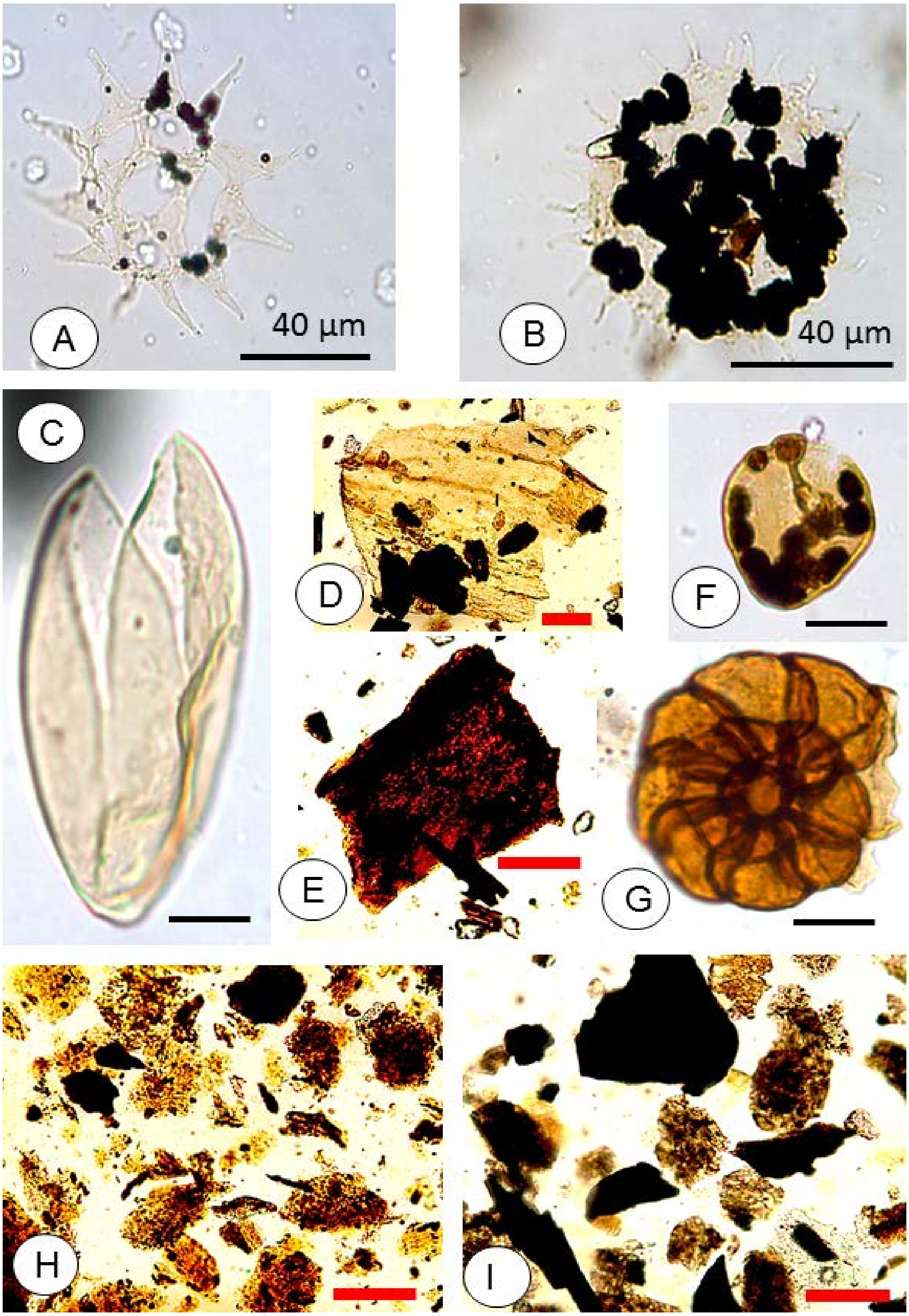

Text-fig. 6. Freshwater algae (A–C), phytoclasts (D, E), pollen (F), Microforaminifera (G) and palynofacies (H, I) of the NDO B-1 well. A, B – *Pediastrum* spp.; A – 49a, 1194 m, 42.3/107.4, B – 44c, 1456 m, 40/103.7, note imprints of pyrite crystals; C – *Ovoidites parvus* (Cookson and Dettmann) Nakoman, 1966; 51c, 1075 m, 52.8/103; D, E – Phytoclasts; D – cuticular sheet, 42a, 1706 m; E – semi-translucent brown wood, 42a, 1706 m; F – Pollen grain showing dark brown aggregate (?Ubisch-like) bodies; 40a, 1792 m, 48.6/101.1; G – Trochospiral microforaminiferal lining; 49b, 1194 m, 30.3/99.8; H – AOM-dominated palynofacies; Sidi Salim Fm., 3, 3675 m; I – Phytoclast-dominated palynofacies; Rosetta Fm., 21, 3035 m. Slide numbers (equivalent to sample numbers), depths (in meters) and microscope co-ordinates are given for every illustrated specimen. Scale bar = 20 µm, unless otherwise indicated.

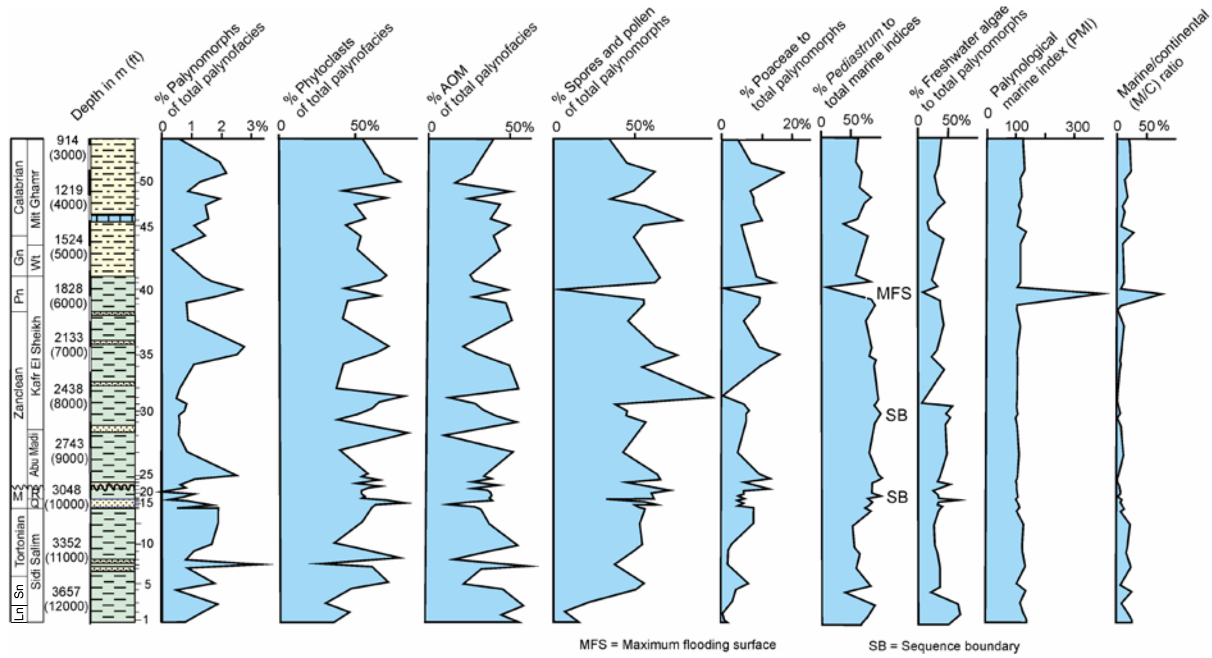

Text-fig. 7. Relative percentage frequency of the main palynofacies categories (palynomorphs, phytoclasts and AOM), selected terrestrial palynomorph groups and the calculated PMI and M/C ratios for the NDO B-1 well. For additional symbols see Text-fig. 3.

Fm.) and 50 (80.9%, Mit Ghamr Fm.). Phytoclasts are visibly less abundant in a few horizons (e.g., 27.9%, sample no. 7, Sidi Salim Fm.). AOM is represented in all samples in appreciable amounts, up to 68.8% of total palynofacies in sample no. 7, where phytoclasts decline (Text-fig. 7). The smallest percentages occur in sample no. 14, (15.8%, Sidi Salim Fm.). Palynomorphs were generally rare (maximum 3.3%, sample no. 7, Sidi Salim Fm.). Pyrite crystals are imprinted over different palynomorph walls in the majority of samples; their abundance was tentatively described as either present or absent.

Palynomorphs

Terrestrial palynomorphs (Text-fig. 4) dominate the palynomorph content, as can be reflected from the low values of the calculated M/C ratio (Text-fig. 7). Spores and pollen were the essential components (up to 94% of total palynomorphs, sample no. 32, depth 2438 m). Spores reach up to 38% of total palynomorphs (sample no. 46, depth 1371 m). Pollen grains were notably abundant (up to 82.5% of total palynomorphs, sample no. 40, depth 1792 m) and were dominated by trilete ferns, with the monolete varieties as minor constituents. Poaceae dominate the pollen association and occur in the majority of samples with percentages up to 20.5% of total palynomorphs (sample no. 51, depth 1075 m), but their abundance declines to 4.2% (sample no. 2, depth 3779 m). Freshwater algae were also important contributors to the NDO B-1 well palynomorphs. At several horizons they reach up to 66.4% of total palynomorphs (sample no. 2, depth 3779 m). Dinoflagellate cysts (Text-fig. 5), along with subordinate microforaminiferal linings, were not as abundant as the pollen and spores. They reach an acme in a single horizon (81.6% of total palynomorphs, sample no. 40, depth 1792 m). Their abundance sometimes declines to 0.5% (sample no. 32, depth 2438 m). The PMI values generally range from 100.5 (sample no. 32, depth 914 m) to 140.7 (sample no. 4, depth 3572 m); an increased value of the index (393.9) was documented at the depth of 1792 m (sample no. 40, near the top of the Kafr El Sheikh Fm.). The M/C ratio was generally low to moderate (0.5 to 28.9), with the exception of a single acme event (74.6) recorded in sample no. 40, corresponding to the highest PMI value.

PALEOENVIRONMENTAL ASSESSMENTS

Tyson (1993, 1995) suggested a potential AOM-phytoclast-palynomorph (APP) ternary plot to pick out the differences in relative proximity to terrestrial organic matter sources, kerogen transport and

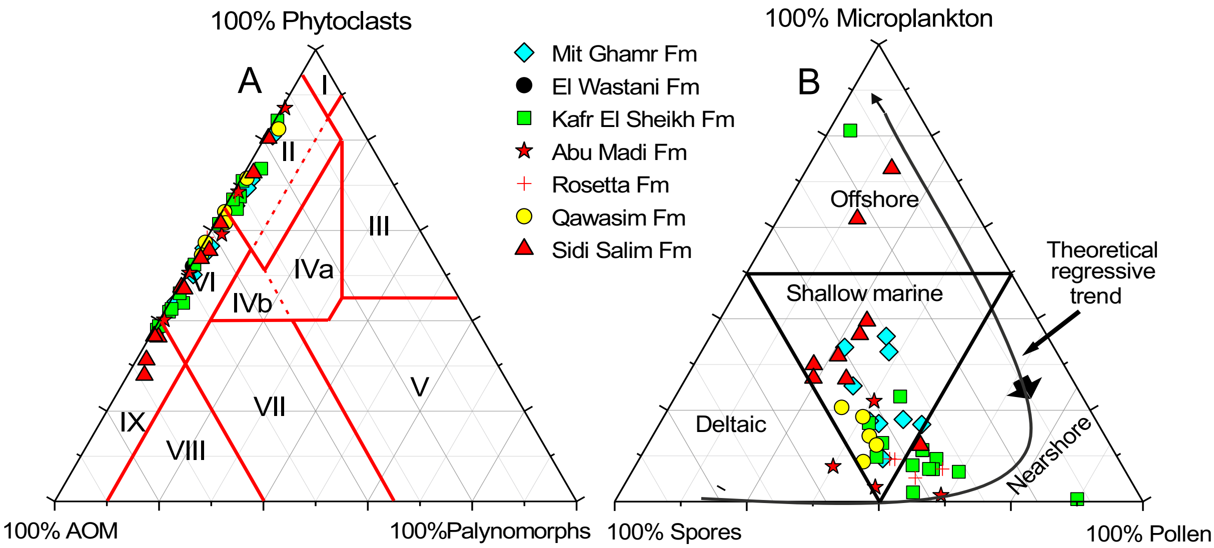

Text-fig. 8. Ternary plots showing the palynologic composition of samples from the NDO B-1 well. A – Microplankton-spore-pollen (MSP) palynomorph diagram (after Federova 1977; Duringer and Doubinger 1985; Traverse 1988); B – AOM-phytoclast-palynomorph kerogen (APP) diagram, based on relative numeric frequencies of main palynofacies components (after Tyson 1993, 1995).

redox states of the sedimentary environments. For the NDO B-1 well, shelfal to basinal environments were inferred from the data plotted on this diagram (Text-fig. 8A). Most samples enter the fields VI and II, which reflects transition from a proximal suboxic-anoxic shelf, with a high AOM content due to reducing conditions, to a marginal dysoxic-anoxic basin, with a diluted AOM content by phytoclasts. Phytoclasts are suggestive of close proximity of, or re-deposition from, fluvio-deltaic sources of the terrestrial organic matter, resulting in dilution of the other palynofacies components, especially palynomorphs. The more distal AOM-dominated suboxic-anoxic basinal settings can be seen in a few horizons of the Sidi Salim and Kafr El Sheikh formations, where samples at these levels enter field IX on the plot (Text-fig. 8A). Higher percentages of AOM may suggest either reducing environments, with a high preservation of autochthonous organic matter, or sedimentation far from active sources of terrestrial matter (Tyson 1995).

Anoxia can be manifested by the occurrence of pyrite in most of the investigated intervals. Roncaglia and Kuijpers (2006) mentioned that pyrite is absent in oxic to dysoxic redox conditions. Pyrite is less common in anoxic fresh to brackish non-marine and hypersaline environments (cf. Batten 1996). In consistence with the pyrite occurrences, oxygen-sensitive dinoflagellate cysts [*Echinidinium* spp., *Lejeunecysta* spp., *Selenopemphix nephroides* (Benedek) Benedek and Sarjeant, 1981, and *Selenopemphix quanta* (Bradford) Matsuoka, 1985] occur in the majority of the samples. This may confirm the existence of anoxic conditions (Zonneveld *et al.* 1997, 2001, 2007). The associated higher percentage frequencies of opaques (oxidized wood and other phytoclasts) in some horizons (Table 1) implies that they might have oxidized during transport and before being transported to the basin. However, at some levels, where pyrite crystals are absent, sensitive dinoflagellate cysts still occur abundantly (e.g., samples nos. 47 to 50, depths 1286–1149 m). In the Mit Ghamr Fm., the low content of such sensitive cysts observed herein conforms to the open marine (distal) settings described by Saleh *et al.* (2024) for the same rock unit, in spite of their interpreted high oxic conditions. Sample no. 2 (depth 3779 m), with plenty of *Selenopemphix* spp. and the moderately sensitive *Spiniferites* spp., is also not consistent with these high oxic states.

Palynofacial and palynological analyses of the examined material suggest, for the majority of the sampling levels, shallow marine (neritic) conditions (Text-figs 7 and 8B). This is indicated by high amounts of terrestrial organic matter that could have been transported to the site of deposition, especially if the latter was influenced by high influx of freshwater river supply. The occurrence of *Spiniferites* spp. in the whole investigated succession (e.g., Text-fig. 5B), along with *Homotryblium* spp. and *Hystrichokolpoma* spp. (Text-fig. 5A, D) are indicative of a typical shelf environment (e.g., Dale 1983; Mahmoud 1998; Carvalho

Sample no.	Depth (m)	Depth (ft)	Formation	Stage (after Makeled *et al.* 2017)	Previous inferred environment: Saleh *et al.* (2024) NDO B-1 well	El-Kahawy *et al.* (2022) onshore Nile Delta	Leila *et al.* (2018) onshore Nile Delta	Shebl *et al.* (2019) Qar'a fields, Nile Delta	Zaghloul *et al.* (2001) northern Nile Delta	Rizzini *et al.* (1978) Nile Delta	Present work (NDO B-1 borehole): redox and environment (after Tyson 1993, 1995)	sensitive dinoflagellate cysts (% of total dinoflagellate cysts)	presence/absence of pyrite	Main dinoflagellate cyst types	Interpreted environment (based on dinoflagellate cysts)
53	856	2810	Mit Ghamr	Calabrian							P	59.7	present	Common to abundant, mainly *Spiniferites, Selenopemphix* and *Lingulodinium*	Open marine (neritic)
52	1030	3380									M	65.0			
51	1075	3530										44.6			
50	1149	3770			Distal (high oxic)										
49	1194	3920									P				
48	1249	4100									M				
47	1286	4220									P				
46	1371	4500			DO								absent	Common, mainly *Spiniferites*	
45	1432	4700			DH							58.0	present	Common to abundant, mainly *Spiniferites, Selenopemphix* and *Lingulodinium*	
44	1456	4780		Gn											
43	1554	5100	W												
42	1706	5600	Kafr El Sheikh	Piazenzian	DO	Middle to outer neritic to upper bathyal			Neritic to basinal	Open sea sediments	M				
41	1770	5810			Distal (high oxic)										
40	1792	5880									P	25.1			
39	1862	6110									M	Not calculated (less than 50 counted dinoflagellate cysts)			Marine (coastal to inner neritic)
38	1889	6200									P				
37	1981	6500		Zanclean											
36	2133	7000									M				
35	2194	7200			PD									Rare to common, mainly *Spiniferites*	
34	2255	7400			DO						P				
33	2375	7795			DH						D				
32	2438	8000			DO						M				
31	2468	8100													
30	2499	8200									P				
29	2560	8400			PS										
28	2590	8500			DO						D				
27	2679	8790	Abu Madi			Restricted (lagoonal)	Continental to marginal marine (estuarine)	Littoral to outer neritic			M				
26	2804	9200			Proximal (dysoxic)						P				
25	2919	9580												Rare, mainly *Spiniferites* and *Lingulodinium*	
24	2926	9600													
23	2956	9700									M				
22	2987	9800									P				
21	3035	9960	Rosetta	Messinian						Fluvio-deltaic	M			Rare to common, mainly *Spiniferites*	
20	3041	9980									P				
19	3048	10000													
18	3066	10060													
17	3072	10080	Qawasim				Prodelta to delta front						absent		
16	3078	10100									M		present		
15	3084	10120													
14	3090	10140									P				
13	3096	10160													
12	3102	10180													
11	3200	10500	Sidi Salim	Tortonian	Distal (oxic)	Middle to outer neritic				Deep sea or outer shelf		18.6	absent	Common to abundant, mainly *Spiniferites, Selenopemphix* and *Lingulodinium*	**Open marine (neritic)**
10	3297	10820									D		present		
9	3340	10960									P		absent		
8	3413	11200									M		present		
7	3432	11260									D	21.4			
6	3444	11300									P				
5	3541	11620		Serra-vallian							M				
4	3572	11720									P	47.1			
3	3675	12060									D				
2	3779	12400		Ln							P	42.0			
1	3797	12460									D	32.3			

D = distal suboxic-anoxic basin P = proximal suboxic-anoxic shelf M = marginal dysoxic-anoxic basin Gn = Gelasian Ln = Langhian
PS = proximal (suboxic) PD = proximal (dysoxic) DO = distal (oxic) DH = distal (high oxic) W = El Wastani Formation

Strong evidence of reworking No information/data

Table 1. List of sample numbers and depths (in m and ft) of the investigated NDO B-1 well succession, indicating current and previous paleoenvironmental determinations in the well and in other onshore-offshore localities of the Nile Delta area. The calculated M/C ratio, the ratio of sensitive to total dinoflagellate cysts and the PMI values are also shown. Brief descriptions of the dinoflagellate cyst types in the succession and a description of pyrite presence/absence are given.

et al. 2016). Brinkhuis (1994) considered that the distribution patterns of *Homotryblium* spp. indicate restricted marine to open marine inner neritic settings. *Spiniferites* spp. has high relative abundances in high productivity areas such as areas influenced by river discharge, but may also occur in oligotrophic sites (see Zonneveld *et al.* 2013). Production of peridinioid cysts *Selenopemphix quanta*, together with gonyaulacoid cysts *Lingulodinium machaerophorum* (Deflandre and Cookson) Wall, 1967 (Text-fig. 5I) and *Spiniferites* spp. (Text-fig. 5B, C and E) increases with the increasing nutrient/trace element availability near river plumes (Zonneveld *et al.* 2009). *Lingulodinium machaerophorum* is restricted to coastal regions and in the vicinity of continental margins; its normal (non-reduced) process lengths in the present samples can be observed in relationship to normal marine salinity (Mertens *et al.* 2009; Zonneveld *et al.* 2009, 2013). Representatives of *Selenopemphix* spp. are restricted to coastal sites. High abundances of *S. quanta* (Text-fig. 5H) occur in eutrophic regions where river discharge waters are present. *S. quanta* can also be transported in large amounts from the shelf into deeper basins (Zonneveld and Brummer 2000), where the upper waters may be either fully-marine or with reduced salinities; its highest relative abundances occur in regions where bottom waters are anoxic to oxic (Zonneveld *et al.* 2013). On the other hand, *S. nephroides* has not been observed in river plume areas; its high relative abundances are observed in mesotrophic-eutrophic environments where bottom waters may be oxic to anoxic (Zonneveld *et al.* 2013). This heterotrophic/autotrophic (phototrophic) dinoflagellate cyst ratio is an excellent proxy for paleoceanographic studies in neritic sequences; its low values may reflect neritic conditions with weak deltaic influence (Matthiessen and Brenner 1996). Although the calculated M/C ratio values in the whole succession are relatively low, their vertical relative variations can provide insights into proximal/distal trends, since this ratio increases from nearshore to offshore environments (e.g., Pellaton and Gorin 2005; Carvalho *et al.* 2013, 2016). In the present case the lowest values of the M/C ratio were documented in the Qawasim, Rosetta, Abu Madi and in the lower Kafr El Sheikh formations (Text-fig. 7), suggesting a regressive trend (coastal to inner neritic environment) for the late Tortonian–early Zanclean interval. The estimated PMI values cannot reflect this vertical environmental development. These shallow marine conditions are reflected by plotting the palynomorph data on the ternary plots of Federova (1977), Duringer and Doubinger (1985) and Traverse (1988), using microplankton-spores-pollen (MSP) as the end-members. Details of the environmental significance of the M/C ratio and PMI are discussed in the following section. For details of current data and previous paleoenvironmental establishments see Table 1.

Poaceae (Gramineae) pollen in the investigated samples possesses variable pollen sizes and is difficult to use alone as a proxy for reconstructing past vegetation and climate (Wei *et al.* 2023), although it is abundant in the fossil records and often used as a paleoclimatic indicator. Unfortunately, there are also problems associated with the morphological similarities across the Poaceae family, which prevent full use of their ecologic preferences. Usually, there are difficulties in visually differentiating between different species of this pollen type (Katsi *et al.* 2024). However, the dominance of Poaceae pollen (Effiom *et al.* 2024) in our samples can be used as evidence of grassy woodlands. A common interpretation is to link the increase in the Poaceae pollen abundance with increasing regional aridity. Poaceae distribution is influenced by various factors, such as the proportion, for example, of the size of local marshes (Bush 2002).

SEQUENCE STRATIGRAPHIC PALYNOMORPH INDICATORS

The chlorococcalean green algae *Pediastrum* spp. (Chlorophyceae), which is frequently and abundantly recorded in the present samples, is indicative of fresh-brackish water lakes, ponds and lagoons and along shores, where water is rich in nutrients; its abundant occurrence indicates a strong influx of freshwater to the depositional environment (Tappan 1980; Batten 1996), since salinity determines its presence/absence (Xiang *et al.* 2021). Adeonipekun *et al.* (2023) have found that the ratio of *Botryoccus*/*Pediastrum*/marine elements is of sequence stratigraphic significance; high proportions were found within lowstand system tracts (LST). According to Helenes *et al.* (1998), the maximum flooding surfaces (MFS) will be usually near the maximum PMI values. However, the patterns of the vertical change in PMI and M/C ratios do not show obvious transgressive/regressive trends. In turn, the calculated PMI values (between 100.5, sample no. 32, depth 914 m to 140.7, sample no. 4, depth 3572 m), seem to reflect an open marine origin of the studied sequence. The palynomorph content documented in sample no. 40 (393.9, depth 1792 m), equivalent to a high M/C ratio (74.6%), indicates a distinct event that stands out from the monotonous palynomorph record. This indicates a rise in the sea level that may correspond to an MFS near the top of the Kafr El Sheikh Fm. Two sequence boundaries (SB) can also be inferred (samples nos. 18, depth 3066 m, basal Rosetta Fm. and 29, depth 2560 m, near the base of the Kafr El Sheikh Fm.), where the highest values of this ratio (97.1 and 98.3, respectively) were observed. However, Helenes *et al.* (1998) distinguished stratigraphic sequences on the basis of calculated PMI values, lithological characteristics and the expression of the wireline logs.

THE MESSINIAN–ZANCLEAN TRANSITION IN THE NDO B-1 WELL

Makled *et al.* (2017, p. 478) defined the base of the Non-distinctive zone (NDZ) in depth interval 3017–3124 m of the NDO B-1 well. This zone represents the interval of time occupied by the Messinian regression event in the Mediterranean area, dated at 5.96–5.332 Ma (Lourens *et al.* 2004). Strata representing this interval in the nearby areas are composed of thin evaporites (Rosetta Fm.) underlain by siliciclastics (Qawasim Fm.), which are the expression of the MSC event. Due to the lack of precise dating within this NDZ in the well (samples nos. 12 to 21, depth interval 3102–3035 m), the recognition of the exact MSC stage(s) is not possible. However, the occurrence of siliciclastics and evaporites most probably favors MSC stage 3 (see Andreetto *et al.* 2021, fig. 1a). Fluvial discharge influence, which characterizes Substage 3.2 'Lago-Mare', can be interpreted by the occurrence of a high percentage of freshwater algae (>24% of total palynomorphs, sample no. 16, depth 3066 m) and land-derived spores (>24% of total palynomorphs, depth 3041 m). The inferred marine (coastal to inner neritic) setting of this interval seems to favor the deep non-desiccated basin hypothesis in the Mediterranean during the MSC (e.g., Roveri *et al.* 2014; Krijgsman *et al.* 2018). These marine conditions during the Messinian fit with the scenario that the Zanclean flooding was effective prior to the Zanclean GSSP (DeCelles and Cavazza 1995; Cavazza and DeCelles 1998). The Zanclean base in the studied succession is well-dated by planktonic foraminifera (Makled *et al.* 2017) and calcareous nannoplankton (Makled and Mandur 2016; Mandur and Makled 2016). In the light of the discovery of vast Messinian terrestrial (riverine) deposits (Madof *et al.* 2019; Menashe River, in the nearby Levant Basin), equivalent sediments in the NDO B-1 well succession (i.e., Qawasim Formation) might have been eroded due to the formation of the well-known widespread regional unconformity (see Shalaby and Sarhan 2023) in the Nile Delta area during the late Messinian. In this case the deep desiccated basin hypothesis (e.g., Hsü *et al.* 1973; Lofi *et al.* 2008; Madof *et al.* 2019) is strongly suggested. For detailed explanation of the controversy concerning the MSC events the reader is kindly referred to Andreetto *et al.* (2021) and discussions/references therein. Pilade *et al.* (2024) recently referred to an example of strong paleoenvironmental change that occurred in the Mediterranean Basin across the Miocene–Pliocene boundary (5.33 Ma) and noted that the paleoenvironmental setting during the Lago-Mare phase of the MSC is still uncertain due to the controversial fossil record of freshwater to brackish and marine assemblages. These authors suggested two scenarios of this strong environmental change, occurring as either a catastrophic/sudden (freshwater to marine) or gradual (brackish to marine) sea level rise. Current data shows that the advent of the Zanclean Stage seems to have been gradual, from coastal/inner neritic to normal open marine (inner to outer neritic) settings.

KEROGEN TYPES AND VISUAL THERMAL MATURATION ASSESSMENT

The content of total organic matter (expressed as total organic carbon, TOC, in wt. %) is important for any given rock unit to produce hydrocarbons. For example, the TOC values of the mudstones and shales in the Qingshankou Fm. of North China (0.21–3.86 wt. %) were considered good source rocks of hydrocarbons (Zhu *et al.* 2023). In a nearby location (Baltim-1 well, about 50 km southeast of the studied well), the measured TOC values range between 0.27–1.18 wt. % in the Sidi Salim, Qawasim and Kafr El Sheikh formations (Saleh *et al.* 2024). Therefore the TOC wt. % content of the investigated sediments can be considered as suitable for producing hydrocarbons.

Visual assessment of the thermal maturity, based on colors of thin-walled spores and pollen, is established in the field of source-rock evaluation and in recognizing the reworking history of the host sediments. Different categories of POM have a potential in producing hydrocarbons and in the resultant hydrocarbon types. AOM is a significant kerogen source of hydrocarbons types I and II, oil-prone source material, whereas phytoclasts make up the bulk composition of kerogen types III and IV, gas-prone to inert source material (e.g., Thompson and Dembicki 1986; Tyson 1995; Batten 1996; Gonçalves

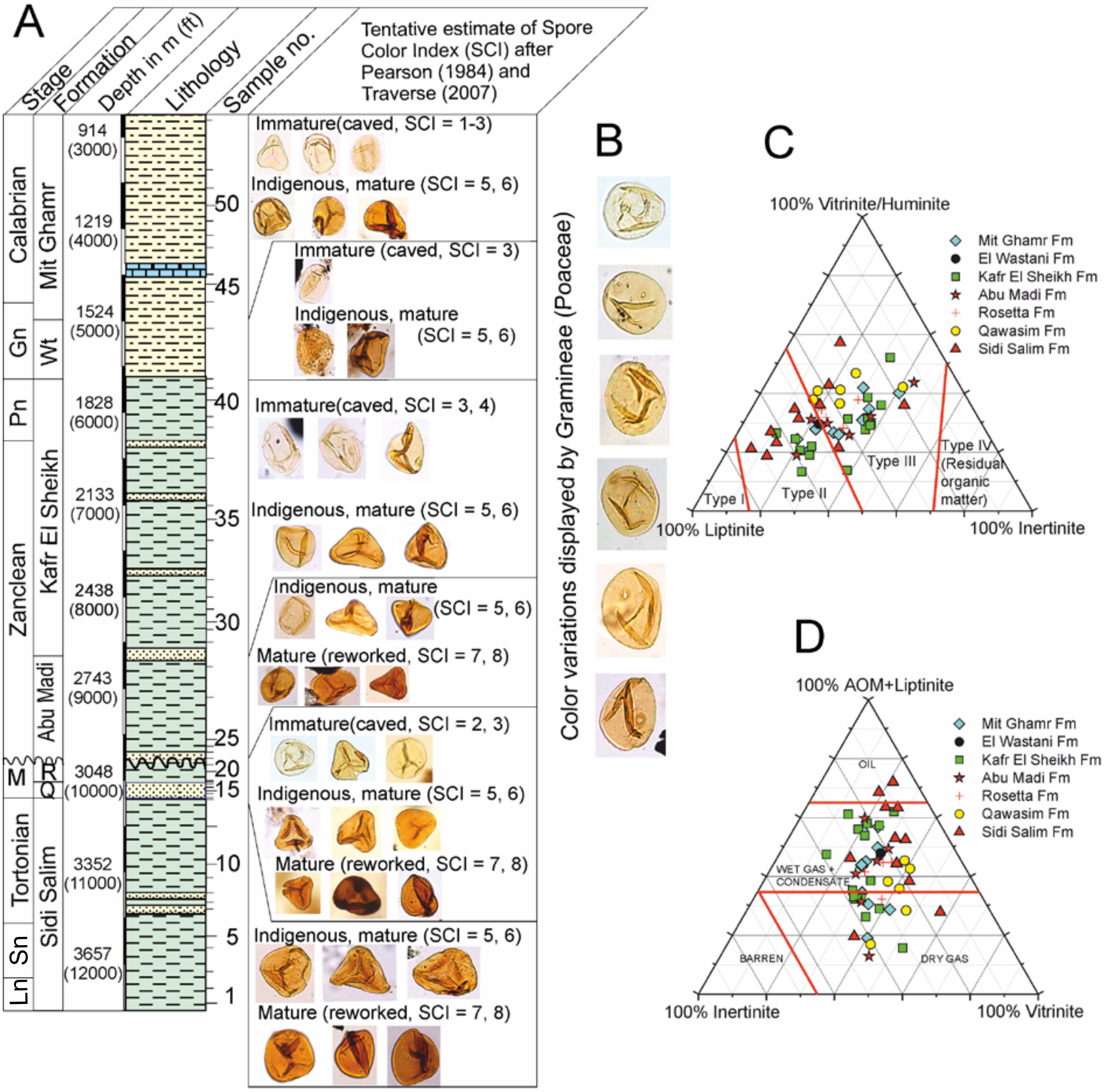

Text-fig. 9. Kerogen types and visual thermal maturation assessment for the analyzed Neogene–Quaternary interval of the NDO B-1 well. A – Spore Color Index (SCI) of thin-walled palynomorphs (mainly trilete spores and partly Poaceae) and their corresponding organic thermal maturity (after Pearson 1984 and Traverse 2007); B – Variable color variations reflected by the encountered Poaceae pollen; C – Ternary Vitrinite / Huminite-Inertinite-Liptinite plot of kerogen types based on major organic components (modified after Cornford 1979); D – Ternary Liptinite-Vitrinite-Inertinite (LVI) kerogen plot (after Dow 1982), with fields indicating predicted hydrocarbon source potential. For additional symbols see Text-fig. 3.

et al. 2015). Suitable reducing conditions are among the favorable conditions for the generation and preservation of organic matter (Wang *et al.* 2024).

The thin-walled palynomorphs, which were usually used to assess SCI, exhibit colors ranging from 1 to 8 (Text-fig. 9A), using the standard color chart adapted after Pearson (1984) and Traverse (2007). Poaceae pollen in this work (Text-fig. 9B) exhibits variable color ranges (SCI = 1–6) and possesses also thin walls, which can enable their effective use in this context. It is suggested that the wide ranges are equivalent to variable maturation states of different geologic ages. We believe that their co-occurrence in the same bed(s) may infer reworked (SCI = 7–8), indigenous (SCI = 5–6, the main assemblage) and caved (SCI = 1–4) palynomorphs. Darker palynomorphs are considered as reworked ones, as can be confirmed by the colors seen in older (Cretaceous) dinoflagellate cysts [e.g., *Cerodinium granulostriatum* (Jain and Millepied) Lentin and Williams, 1987] and pollen [e.g., *Afropollis jardinus* (Brenner) Doyle, Jardiné and Doerenkamp, 1982]. Taxonomically, these palynofossils are easily recognizable from the Neogene–Quaternary associations. The degree of how this reworking may have influenced our assemblages remains enigmatic. Plotting the Neogene–Quaternary samples from the NDO B-1 well succession on the ternary diagram of Cornford (1979) reflects types II and III kerogen (Text-fig. 9C). Exceptionally, the Qawasim and Rosetta formations reveal only type III kerogen. According to Tyson (1995), types II and III are oil- and gas-prone, respectively. However, on the ternary plot of Dow (1982) (Text-fig. 9D), samples show only dry gas or wet gas/condensates. In the light of the above-mentioned discussions, the succession is considered thermally mature and capable of producing hydrocarbons.

CONCLUSIONS

Based on the palynomorph and palynofacies analyses of the Neogene to Quaternary succession from the NDO B-1 well, drilled in the offshore Nile Delta (Egypt), open marine (neritic) environments were inferred for the Sidi Salim, upper Kafr El Sheikh, El Wastani and Mit Ghamr formations. Relatively shallower environments (coastal to inner neritic) were interpreted for the Qawasim, Rosetta and the lower Kafr El Sheikh formations. The nature and composition of the total POM reflects open marine (neritic) environmental conditions during deposition of the majority of the investigated sediments. This marine setup is documented by the occurrence of dinoflagellate cysts, along with microforaminiferal linings, across the whole investigated succession. The occurrence of pyrite, imprinted on several palynomorphs, and sensitive to moderately sensitive dinoflagellate cysts to oxygen degradation (*Selenopemphix* and *Spiniferites*, respectively) supports a reducing state. The highest value of the PMI, equivalent to the highest M/C ratio, indicates a significant rise in sea level (i.e. the development of MFS) near the top of Kafr El Sheikh Fm. The generalized lower values of the M/C ratio may be attributed to the large influx of the Nile River, in which marine phytoplankton was diluted by the land-derived spores/pollen and freshwater algae. In this case, the low abundance of dinoflagellate cysts can hardly be applied to track the relative sea level changes. Our palynofacies and palynological findings do not confirm the previously inferred distal environments at the top of the Abu Madi Fm., or the high oxic states at some levels of the Kafr El Sheikh, El Wastani and Mit Ghamr formations. The vertical development of environment, from neritic, coastal/inner neritic to neritic, suggests that the advent of Zanclean Stage (basal Abu Madi Fm.) witnessed gradual, non-drastic restoration of normal marine conditions. The absence of the MSC stages 1 and 2 and the occurrence of a widespread Messinian/Zanclean unconformity may suggest a near-desiccated Mediterranean Sea during the Messinian time. From a sequence stratigraphic point of view, an MFS near the top of the Kafr El Sheikh Fm. is also suggested. Moreover, the highest values of *Pediastrum* (high *Pediatrum*/marine elements ratio) may reflect two sequence boundaries at the base of Rosetta Fm. and near the base of the Kafr El Sheikh Fm. The investigated organic matter is mature and generative of dry gas and wet gas/condensates. Reworked Cretaceous dinoflagellate cysts (e.g., *Cerodinium granulostriatum*) and pollen grains (e.g., *Afropollis jardinus*) were seen in the upper Sidi Salim, Qawasim and Rosetta formations. Reworking can be confirmed by the presence of older and relatively darker palynomorphs, which are distinctive from indigenous palynomorphs.

Acknowledgements

The authors are deeply indebted to the Egyptian General Petroleum Corporation (E.G.P.C), for providing the samples and well logs for this study. We greatly thank Marcin Barski, an anonymous reviewer and the AGP editor Anna Żylińska, for their valuable comments and remarks which improved the quality of the manuscript.

REFERENCES

Adeonipekun, P.A., Adeleye, M.A., Adebay, M.B. and Sowunmi, M.A. 2023. The potentials of accessory palynomorphs as sequence stratigraphic and basin evaluation tools in the shallow offshore Niger Delta. *Review of Palaeobotany and Palynology*, **318**, 104985.

Aksu, A.E., Hall J. and Yaltırak, C. 2005. Miocene to Recent tectonic evolution of the eastern Mediterranean: New pieces of the old Mediterranean puzzle. *Marine Geology*, **221**, 1–13.

Andreetto, F., Aloisi G., Raad, F., Heida, H., Flecker, R., Agiadi, K., Lofi, J., Blondel, S., Bulian, F., Camerlenghi, A., Caruso, A., Ebner, R., Garcia-Castellanos, D., Gaullier, V., Guibourdenche, L., Gvirtzman, Z., Hoyle, T.M., Meijer, P.T., Moneron, J., Sierro, F.J., Travan, G., Tzevahirtzian, A., Vasiliev, I. and Krijgsman, W. 2021. Freshening of the Mediterranean Salt Giant: controversies and certainties around the terminal (Upper Gypsum and Lago-Mare) phases of the Messinian Salinity Crisis. *Earth-Science Reviews*, **216**, 103577.

Batten, D.J. 1996. Palynofacies and palaeoenvironmental interpretation. In: Jansonius, J. and McGregor, D.C. (Eds), Palynology: Principles and Applications, 1011–1064. American Association of Stratigraphic Palynologists Foundation; Dallas.

Benedek, P.N. and Sarjeant, W.A.S. 1981. Dinoflagellate cysts from the Middle and Upper Oligocene of Tönisberg (Niederrheingebiet): a morphological and taxonomic restudy. *Nova Hedwigia*, **35**, 313–356.

Brinkhuis, H. 1994. Late Eocene to Early Oligocene dinoflagellate cysts from the Priabonian type-area (Northeast Italy): biostratigraphy and paleoenvironmental interpretation. *Palaeogeography. Palaeoclimatology, Palaeoecology*, **107**, 121–163.

Bujak, J.P., Downie, C., Eaton, G.L. and Williams, G.L. 1980. Dinoflagellate cysts and acritarchs from the Eocene of southern England. *Special Papers in Palaeontology*, **24**, 1–100.

Bush, M.B. 2002. On the interpretation of fossil Poaceae pollen in the lowland humid neotropics. *Palaeogeography, Palaeoclimatology, Palaeoecology*, **177**, 5–17.

Carvalho, M.A., Bengtson, P. and Lana, C.C. 2016. Late Aptian (Cretaceous) paleoceanography of the South Atlantic Ocean inferred from dinocyst communities of the Sergipe Basin, Brazil, *Paleoceanography*, **31**, 2–26.

Carvalho, M.A., Ramos, R.R.C., Crud, M.B., Witovisk, L., Kellner, A.W.A., Silva, H.P., Grillo, O.N., Riff, D. and Romano, P.S. 2013. Palynofacies as indicators of paleoenvironmental changes in a Cretaceous succession from the Larsen Basin, James Ross Island, Antarctica. *Sedimentary Geology*, **295**, 53–66.

Cavazza, W. and DeCelles, P.G. 1998. Upper Messinian siliciclastic rocks in southeastern Calabria (southern Italy): paleotectonic and eustatic implications for the evolution of the central Mediterranean region. *Tectonophysics*, **298**, 223–241.

Cita, M.B. 1973. Pliocene biostratigraphy and chronostratigraphy. *Initial Reports of the Deep Sea Drilling Project*, **13**, 1343–1379.

Cornford, C. 1979. Initial Reports of the Deep-Sea Drilling Project. Part. 1, 503–510. US Government Printing Office; Washington.

Dale, B. 1983. Dinoflagellate resting cysts: 'benthic plankton'. In: Fryxel, G.A. (Ed.), Survival strategies of the algae, 69–136. Cambridge University Press; Cambridge.

Deaf, A.S., Tahoun, S.S., Gentzis, T., Carvajal-Ortiz, H., Harding, I.C., Marshall, J.E.A. and Ocubalidet, S. 2020. Organic geochemical, palynofacies, and petrographic analyses examining the hydrocarbon potential of the Kharita Formation (Albian) in the Matruh Basin, northwestern Egypt. *Marine and Petroleum Geology*, **112**, 104087.

DeCelles, P. and Cavazza, W. 1995. Upper Messinian fanglomerates in eastern Calabria (southern Italy): response to microplate migration and Mediterranean sea-level changes. *Geology*, **23**, 775–778.

Dow, W.G. 1982. Kerogen maturity and type by reflected light microscopy applied to petroleum exploration. In: Staplin, F.L., Dow, W.G., Milner, C.W.O., Milner, C.W.D., O'Connor, D.I., Pocock, S.A.J., Van Gijzel, P., Welte, D.H. and Yukler, M.A. (Eds), How to assess Maturation and Paleotemeratures. *Society of Economic Paleontologists and Mineralogists Short Course*, **7**, 133–157.

Doyle, J.A., Jardiné, S. and Doerenkamp, A. 1982. *Afropollis*, a new genus of early angiosperm pollen, with notes on the Cretaceous palynostratigraphy and paleoenvironments of Northern Gondwana. *Bulletin des Centres de Recherches Exploration-Production Elf-Aquitaine*, **6** (1), 39–117.

Duringer, P. and Doubinger, J. 1985. La palynologie: un outil de caractérisation des faciès marins et continentaux à la limite Muschelkalk supérieur-Lettenkohle. *Sciences Géologiques, bulletins et mémoires*, **38**, 19–34.

E.G.P.C. 1994. Western Desert, oil and gas fields (a comprehensive overview), 431 pp. Egyptian General Petroleum Corporation; Cairo.

Effiom, A.C., Neumann, F.H., Bamford, M.K. and Scott, L. 2024. Mid–Late Holocene palynological development at Lake St Lucia, KwaZulu-Natal. *Review of Palaeobotany and Palynology*, **322**, 105046.

Eisawi, A. and Schrank, E. 2008. Upper Cretaceous to Neogene palynology of the Melut Basin, southeast Sudan. *Palynology*, **31** (1), 101–129.

El Atfy, H. 2021. Palynofacies as a paleoenvironment and hydrocarbon source potential assessment tool: An example from the Cretaceous of north Western Desert, Egypt. *Palaeobiodiversity and Palaeoenvironments*, **101**, 35–50.

El Diasty, W.S., El Beialy, S.Y., El Attar, R.M., Khairy, A., Peters, K.E. and Batten, D.J. 2019. Oil source correlation in the West Esh El Mellaha, southwestern margin of the Gulf of Suez rift, Egypt. *Journal of Petroleum Science Engineering*, **180**, 844–860.

El-Kahawy, R. M., Aboul-Ela, N., El-Barkooky, A.N. and Kassab, W. 2022. Biostratigraphy and paleoenvironment implications of the Middle Miocene–Early Pliocene succession, El-Wastani gas field, onshore Nile Delta, Egypt. *Arabian Journal of Geosciences*, **15**, 341.

El Nady, M.M. and. Harb, F.M. 2010. Source rocks evaluation of Sidi Salem-1 well in the onshore Nile Delta, Egypt. *Petroleum Science and Technology*, **28** (14), 1492–1502.

Federova, V.A. 1977. The significance of the combined use of microphytoplankton, spores, and pollen for differentiation of multi-facies sediments. In Samoilovich, S.R, and Timoshina, N.A. (Eds), Questions of Phytostratigraphy. *Trudy, Neftyanoi nauchnoissledovatelskii geologorazvedochnyi Institut (VNIGRI)*, **398**, 70–88. [In Russian]

Gonçalves, P.A., da Silva, T.F., Mendonça Filho, J.G. and Flores, D. 2015. Palynofacies and source rock potential of Jurassic sequences on the Arruda sub-basin (Lusitanian Basin, Portugal). *Marine and Petroleum Geology*, **59**, 575–592.

Hamouda, A. and El-Gharabawy, S. 2019. Impacts of neotectonics and salt diapir on the Nile fan deposit, Eastern Mediterranean. *Environmental and Earth Sciences Research Journal*, **6** (1), 8–18.

Helenes, J., De-Guerra, C. and Vasquez, J. 1998. Palynology and chronostratigraphy of the upper Cretaceous in the subsurface of the Barinas area, western Venezuela. *American Association of Petroleum Geologists Bulletin*, **82**, 1308–1328.

Hsü, K.J., Cita, M.B. and Ryan, W.B.F. 1973. The origin of the Mediterranean evaporites. *Initial Reports of the Deep Sea Drilling Project*, **13** (2), 1203–1231.

Katsi, F., Kent, M.S., Jones, M., Fraser, W.T., Jardine, P.E., Eastwood, W., Mariani, M., Osborne, C., Edwards, S. and Lomax, B.H. 2024. FTIR spectra from grass pollen: A quest for species-level resolution of Poaceae and Cerealia-type pollen grains. *Review of Palaeobotany and Palynology*, **321**, 105039.

Krijgsman, W., Capella, W., Simon, D., Hilgen, F.J., Kouwenhoven, T.J., Meijer, P.Th., Sierro, F.J., Tulbure, M.A., van den Berg, B.C.J., van der Schee, M. and Flecker, R. 2018. The Gibraltar Corridor: watergate of the Messinian Salinity Crisis. *Marine Geology*, **403**, 238–246.

Leila, M., Moscariello, A. and Šegvić, B. 2019. Depositional facies controls on the diagenesis and reservoir quality of the Messinian Qawasim and Abu Madi formations, onshore Nile Delta, Egypt. Geological Journal, **54**, 1797–1813.

Leila, M., Sen, S., Ganguli, S.S. and Abioui, M. 2023. Integrated petrographical and petrophysical evaluation for reservoir management of the upper Miocene Qawasim sandstones in west Dikirnis, onshore Nile Delta, Egypt. *Geoenergy Science and Engineering*, **226**, 211789.

Lentin, J.K. and Williams, G.L. 1987. Status of the fossil dinoflagellate genera *Ceratiopsis* Vozzhennikova 1963 and *Cerodinium* Vozzhennikova 1963 emend. *Palynology*, **11**, 113–116.

Lofi, J., Deverchère, J., Gaullier, V., Gillet, H., Gorini, C., Guennoc, P., Loncke, L., Maillard, A., Sage, F., Thinon, I., Capron, A. and Obone Zue Obame, E. 2008. The Messinian Salinity Crisis in the offshore domain: an overview of our knowledge through seismic profile interpretation and multi-site approach. In: Briand, F. (Ed.), The Messinian Salinity Crisis from mega-deposits to microbiology – A consensus report, 83–90. CIESM; Monaco.

Lourens, L.J., Hilgen, F.J., Shackleton, N.J., Laskar, J. and Wilson, D. 2004. Appendix 2. Orbital tuning calibration and conversions for the Neogene Period. In: Gradstein, F.M., Ogg, J.G. and Smith, A.G. (Eds), A Geologic Time Scale 2004, 469–484. Cambridge University Press; Cambridge.

Madof, A.S., Bertoni, C. and Lofi, J. 2019. Discovery of vast fluvial deposits provides evidence for drawdown during the late Miocene Messinian salinity crisis. *Geology*, **47**, 171–174.

Mahmoud, M.S. 1998. Palynology of Middle Cretaceous–Tertiary sequence of Mersa Matruh-1 well, northern Western Desert, Egypt. *Neues Jahrbuch für Geologie und Paläontologie, Abhandlungen*, **209** (1), 79–104.

Mahmoud, M.S. and Khalaf, M.M. 2023. Paleoenvironmental contribution and visual kerogen assessment of some Upper Cretaceous sediments from southern Egypt. *Arabian Journal of Geosciences*, **16**, 375.

Makled, W.A. and Mandur, M.M.M. 2016. Nannoplankton calendar: applications of nannoplankton biochronology in sequence stratigraphy and basin analysis in the subsurface offshore Nile Delta, Egypt. *Marine and Petroleum Geology*, **72**, 374–392.

Makled, W.A., Mandur, M.M. and Langer, M.R. 2017. Neogene sequence stratigraphic architecture of the Nile Delta, Egypt: a micropaleontological perspective. *Marine and Petroleum Geology*, **85**, 117–135.

Mandur, M.M.M. and Makled, W.A. 2016. Implications of calcareous nannoplankton biostratigraphy and biochronology of the Middle–Late Miocene of the Nile Delta, Egypt. *Arabian Journal of Geosciences*, **9**, 203.

Matsuoka, K. 1985. Organic-walled dinoflagellate cysts from surface sediments of Nagasaki Bay and Senzaki Bay, west Japan. *Faculty of Liberal Arts, Nagasaki University, Natural Science, Bulletin*, **25** (2), 21–115.

Matthiessen, J. and Brenner, W. 1996. Dinoflagellate cyst ecostratigraphy of Pliocene–Pleistocene sediments from the Yermak Plateau (Arctic Ocean, Hole 911A). Proceedings of the Ocean Drilling Program, Science Results, **151**, 243–253.

Mertens, K., Ribeiro, S., Bouimatarhan, I., Caner, H., Combourieu-Nebout, N., Dale, B., De Vernal, A., Ellegaard, M., Filipova, M., Godhe, A., Goubert, E., Grøsfjeld, K., Holzwarth, U., Kotthoff, U., Leroy, S.A.G., Londeix, L., Marret, F., Matsuoka, K., Mudie, P.J., Naudts, L., Peña-Manjarrez, J.-L., Persson, A., Popescu, S.-M., Pospelova, V., Sangiorgi, F., van der Meer, T.J., Vink, A., Zonneveld, K.A.F., Vercauteren, D., Vlassenbroeck, J. and Louwye, S. 2009. Process length variation in cysts of a dinoflagellate, *Lingulodinium machaerophorum*, in surface sediments and its potential use as a salinity proxy. *Marine Micropalaeontology*, **70**, 54–69.

Metwalli, F.I., Ismail, A., Metwally, M.S. and El Shafei, I.M. 2023. Sequence stratigraphic evaluation for the Abu Madi Formation, Abu Madi/El Qar'a/Khilala gas fields, onshore Nile Delta, Egypt. *Petroleum Research*, **8**, 514–523.

N.C.G.S. 1976. Miocene rock stratigraphy of Egypt. *Egyptian Journal of Geology*, **18** (1), 1–69.

Nabawy, B.S., Abd El Aziz, E.A., Ramadan, M. and Shehata, A.A. 2023. Implication of the micro- and lithofacies types on the quality of a gas-bearing deltaic reservoir in the Nile Delta, Egypt. *Scientific Reports*, **13**, 8873.

Nakoman, E. 1966. Contribution à l'étude palynologique des formations tertiaries du basin de Thrace. I. *Annales de la Société Géologique du Nord*, **86**, 65–107.

Ouda, Kh. and Obaidalla, N. 1995. The geologic evolution of the Nile Delta area during the Oligocene–Miocene. *Egyptian Journal of Geology*, **39** (1), 77–111.

Pearson, D.L. 1984. Pollen/spore color 'standard', 3 pp. Phillips Petroleum Company Exploration Projects Section, Geological Branch; Bartlesville, Oklahoma.

Pellaton, C. and Gorin, G.E. 2005. The Miocene New Jersey passive margin as a model for the distribution of sedimentary organic matter in siliciclastic deposits. *Journal of Sedimentary Research*, **75** (6), 1011–1027.

Pilade, F., Licata, M., Vasiliev, I., Birgel, D., Dela Pierre, F., Natalicchio, M., Mancini, A., Mulch, A. and Gennari, R. 2024. Probing large paleoenvironmental variability of Mediterranean during the Miocene–Pliocene transition via advanced multivariate statistical analysis on lipid biomarker multiproxy. EGU General Assembly 2024, Vienna, Austria, 14–19 Apr 2024, EGU24-399.

Potonié, R. 1960. Sporologie der eozänen Kohle von Kalewa in Burma. *Senckenbergiana lethaea*, **41**, 451–481.

Rizzini, A., Vessani, F., Cococetta, V. and Milad, G. 1978. Stratigraphy and sedimentation of Neogene–Quaternary section in the Nile Delta area. *Marine Geology*, **27**, 327–348.

Roncaglia, L. and Kuijpers, A. 2006. Revision of the palynofacies model of Tyson (1993) based on recent high-latitude sediments from the North Atlantic. *Facies*, **52**, 19–39.

Roveri, M., Manzi, V., Bergamasco, A., Falcieri, F.M., Gennari, R., Lugli, S., and Schreiber, B.C. 2014. Dense water cascading and Messinian canyons: A new scenario for the Mediterranean salinity crisis. *American Journal of Science*, **314**, 751–784.

Sah, S.C.D. 1967. Palynology of an Upper Neogene profile from Rusizi Valley (Burundi), 173 pp. Musée Royal de l'Afrique Centrale; Tervuren.

Saleh, R.A., Makled, W.A., Moustafa, T.F., Aboul Ela, N.M. and Tahoun, S.S. 2024. Depositional phases of Neogene rocks based on palynofacies and inorganic geochemical analyses in Nile Delta, Egypt: A focus on organic matter accumulation. *Journal of African Earth Sciences*, **209**, 105105.

Sarhan, M.A., Collier, R., Basal, A. and Abdel Aal, M.H. 2014. Late Miocene normal faulting beneath the northern Nile Delta: NNW propagation of the Gulf of Suez Rift. *Arabian Journal of Geosciences*, **7**, 4563–4571.

Sestini, G. 1995. Egypt. In: Kulke, H. (Ed.), Regional Petroleum Geology of the World, Part II: Africa, America, Australia and Antarctica. *Beitrage zur regionalen Geologie der Erde*, **22**, 57–87. Bornträger; Stuttgart.

Shalaby, A. and Sarhan, M.A. 2023. Pre- and post-Messinian deformational styles along the northern Nile Delta Basin in the framework of the Eastern Mediterranean tectonic evolution. *Marine Geophysical Research*, **44**, 22.

Shebl, S., Ghorab, M., Mahmoud, A., Shazly, T., Abuhagaza, A.A. and Shibl, A. 2019. Linking between sequence stratigraphy and reservoir quality of Abu Madi Formation utilizing well logging and seismic analysis at Abu Madi and El Qar'a fields, Nile Delta, Egypt. *Egyptian Journal of Petroleum*, **28**, 213–223.

Stover, L.E. and Evitt, W.R. 1978. Analyses of pre-Pleistocene organic-walled dinoflagellates. *Stanford University Publications, Geological Sciences*, **15**, 1–300.

Tappan, H. 1980. The Paleobiology of Plant Protists, 1028 pp. Freeman; San Francisco.

Thompson, C.L. and Dembicki, H. Jr. 1986. Optical characteristics of amorphous kerogens and hydrocarbon-generating potential of source rocks. *International Journal of Coal Geology*, **6**, 229–249.

Traverse, A. 1988. Paleopalynology, 600 pp. Unwin Hyman; Boston.

Traverse, A. 2007. Paleopalynology, 813 pp. Springer; Dordrecht.

Tyson, R.V. 1993. Palynofacies analysis. In: Jenkins, D.J. (Ed.), Applied Micropalaeontology, 153–191. Kluwer Academic Publishers; Dordrecht.

Tyson, R.V. 1995. Sedimentary organic matter: organic facies and palynofacies, 615 pp. Chapman and Hall; London.

Wall, D. 1967. Fossil microplankton in deep-sea cores from the carribean. *Palaeontology*, **10** (1), 95–123.

Wang, X., Zhu, X., Lai, J., Lin, X., Wang, X., Du, Y., Huang, C. and Zhu, Y. 2024. Paleoenvironmental reconstruction and organic matter accumulation of the Paleogene Shahejie oil shale in the Zhanhua Sag, Bohai Bay Basin, Eastern China. *Petroleum Science*, **21** (3), 1552–1568.

Wei, C., Jardine, P.E., Gosling, W.D. and Hoorn, C. 2023. Is Poaceae pollen size a useful proxy in palaeoecological studies? New insights from a Poaceae pollen morphological study in the Amazon. *Review of Palaeobotany and Palynology*, **308**, 104790.

Xiang, L., Huang, X., Huang, C., Chen, X., Wang, H., Chen, J., Hu, Y., Sun, M. and Xiao, Y. 2021. *Pediastrum* (Chlorophyceae) assemblages in surface lake sediments in China and western Mongolia and their environmental significance *Review of Palaeobotany and Palynology*, **289**, 104396.

Zaghloul, Z.M., Elgamal, M.M., El Araby, H. and Abdel Wahab, W. 2001. Evidences of geotectonic and ground motions in the Northern Nile Delta. In: Zaghloul, Z. and Elgamal, M.M. (Eds), Deltas: modern and ancient, 285–314. Mansoura University; Cairo.

Zhu, X., Cao, J., Xia, L., Bian, L., Liu, J. and Zhang, R. 2023.

Links between marine incursions, lacustrine anoxia and organic matter enrichment in the Upper Cretaceous Qingshankou Formation, Songliao Basin, China. *Marine and Petroleum Geology*, **158** (A), 106536.

Zonneveld, K.A.F., Bockelmann, F. and Holzwarth, U. 2007. Selective preservation of organic walled dinoflagellate cysts as a tool to quantify past net primary production and bottom water oxygen concentrations. *Marine Geology*, **237**, 109–126.

Zonneveld, K.A.F. and Brummer, G.J.A. 2000. (Palaeo-)ecological significance, transport and preservation of organic-walled dinoflagellate cysts in the Somali Basin, NW Arabian Sea. *Deep Sea Research, Part II: Topical Studies in Oceanography*, **47**, 2229–2256.

Zonneveld, K.A.F., Chen, L., Möbius, J. and Mahmoud, M.S. 2009. Environmental significance of dinoflagellate cysts from the proximal part of the Po-river discharge plume (off southern Italy, Eastern Mediterranean). *Journal of Sea Research*, **62**, 189–213.

Zonneveld, K.A., Marret, F., Versteegh, G.J.M., Bogus, K., Bonnet, S., Bouimetarhan, I., Crouch, E., de Vernal, A., Elshanawany, R., Edwards, L., Esper, O., Forke, S., Grøsfjeld, K., Henry, M., Holzwarth, U., Kielt, J.-F., Kim, S.-Y., Ladouceur, S., Ledu, D., Chen, L., Limoges, A., Londeix, L., Lu, S.-H., Mahmoud, M.S., Marino, G., Matsouka, K., Matthiessen, J., Mildenhal, D.C., Mudie, P., Neil, H.L., Pospelova, V., Qi, Y., Radi, T., Richerol, T., Rochon, A., Sangiorgi, F., Solignac, S., Turon, J.-L., Verleye, T., Wang, Y., Wang, Z. and Young, M. 2013. Atlas of modern dinoflagellate cyst distribution based on 2405 datapoints. *Review of Palaeobotany and Palynology*, **191**, 1–197.

Zonneveld, K.A.F., Versteegh, G.J.M. and De Lange, G.J. 1997. Preservation of organic walled dinoflagellate cysts in different oxygen regimes: a 10,000 year natural experiment. *Marine Micropaleontology*, **29**, 393–405.

Zonneveld, K.A.F., Versteegh, G.J.M. and De Lange, G.J. 2001. Palaeoproductivity and postdepositional aerobic organic matter decay reflected by dinoflagellate cyst assemblages of the Eastern Mediterranean S1 sapropel. *Marine Geology*, **172**, 181–195.

Manuscript submitted: 12th May 2024
Revised version accepted: 19th August 2024

Appendix 1

List of the counted palynofacies categories from the NDO B-1 well used in this study.

			Palynomorphs					Phytoclasts									
Sample no.	Depth (m)	Depth (ft)	Spores	Pollen	Dinoflagellate cysts	Microforaminifera linings	Total palynomorphs	Brown wood phytoclasts	Degraded wood	Tracheids	Cuticles	Membranous tissues	Fungal hyphens	Opaque phytoclasts	Total phytoclasts	AOM	TOTAL PALYNOFACIES
53	856	2810		3			3	106	28	4				159	297	230	530
52	1030	3380	5	6			11	117	32	15	1	6		191	362	180	553
51	1075	3530	5	7			12	144	39			5		188	376	154	542
50	1149	3770	4	3			7	187	24		1	3	2	220	437	96	540
49	1194	3920	2	3			5	89	26	11		4	1	100	231	300	536
48	1249	4100	3	7		1	11	147	58	15	2	5	2	160	389	146	546
47	1286	4220	1	5	2		8	113	27	7	1	4	1	123	276	266	550
46	1371	4500	1	8			9	95	47	3		4		170	319	236	564
45	1432	4700		5	1		6	59	45	2		2		127	235	290	531
44	1456	4780	2	5	1		8	108	21	2	3	9	2	153	298	237	543
43	1554	5100		2			2	93	51	8		7		120	279	255	536
42	1706	5600	1	2			3	147	55		7	7	1	181	398	160	561
41	1770	5810	1	7	1		9	106	41	6		3	1	198	355	161	525
40	1792	5880		7	7	1	15	76	23	3		5		140	247	300	562
39	1862	6110	7	3			10	131	28	5		10	3	200	377	172	559
38	1889	6200	2	3			5	92	17	3		4	2	129	247	284	536
37	1981	6500	2	2	1		5	73	26	7		4	2	116	228	310	543
36	2133	7000	5	9	1		15	140	39		4	11	2	204	400	128	543
35	2194	7200	5	9	1		15	122	30		5	3	1	215	376	190	581
34	2255	7400	2	3	1		6	107	15	3		7	1	98	231	305	542
33	2375	7795	1	2			3	122	12	1			1	59	195	315	513
32	2438	8000	1	2			3	204	78	7	1	3		180	473	85	561
31	2468	8100		4			4	127	17	6		3		198	351	170	525
30	2499	8200	2	2			4	130	30		1	5		159	325	200	529
29	2560	8400	1	2			3	48	19	6		1		205	279	250	532
28	2590	8500	1	2			3	55	14			1	1	134	205	320	528
27	2679	8790	1	2			3	148	63	8		7	1	225	452	64	519
26	2804	9200	1	4			5	68	22	6	1	6		115	218	319	542
25	2919	9580	6	6	1		13	96	28		4	6	2	175	311	202	526
24	2926	9600	2	4			6	94	51	5		4	2	130	286	231	523
23	2956	9700	2	2		1	5	105	53		2	4	6	192	362	161	528
22	2987	9800		3			3	97	55		2	10	2	103	269	260	532
21	3035	9960	1	3			4	124	72	1	1	3		159	360	168	532
20	3041	9980					0	153	3					168	324	230	554
19	3048	10000	1	5			6	147	18	3				123	291	230	527
18	3066	10060	1	3			4	141	34	9				111	295	235	534
17	3072	10080		1			1	205	5	2				85	297	220	518
16	3078	10100		4	1		5	128	86		2		1	95	312	255	572
15	3084	10120		5	2		7	271	32	4	1			162	470	180	657
14	3090	10140	3	6			9	157	53	3				224	437	84	530
13	3096	10160		3			3	209	21	8	1			133	372	205	580
12	3102	10180	1	10			11	152	42	13	4		2	146	359	212	582
11	3200	10500		9	1		10	112	82				1	105	300	230	540
10	3297	10820	1	7	1		9	90	27		2	3	2	70	194	330	533
9	3340	10960	1	4	1		6	40	74		3			175	292	245	543
8	3413	11200		4			4	111	69	2		5	4	235	426	100	530
7	3432	11260	8	8	1		17	68	33		3	1	6	35	146	360	523
6	3444	11300		5			5	116	94	5	1	11	2	100	329	200	534
5	3541	11620	4	4	1		9	172	112		7	4	1	77	373	131	513
4	3572	11720		2	1		3	158	21		7	3	1	70	260	285	548
3	3675	12060	2	6	2		10	18	78		1			65	162	345	517
2	3779	12400	2	4	1		7	93	61		1	2	6	81	244	268	519
1	3797	12460	1	1	2		4	12	123		5			50	190	325	519

Appendix 2

List of the counted palynomorph groups from the NDO B-1 well used in this study (samples with poor recovery were ignored).

Sample no.	Depth (m)	Depth (ft)	Trilete spores	Monolete spores	Fungal spores	Poaceae (Gramineae) pollen	Bisaccate pollen	Other pollen	Total spores and pollen	*Ovoidites*/*Schizosporis* spp.	*Pediastrum* spp.	Other freshwater algae	Total Freshwater algae	Total terrestrial palynomorphs	Dinoflagellate cysts	Microforaminifera linings	Total marine palynomorphs	TOTAL PALYNOMORPHS
53	856	2810	38	0	16	17	2	40	113	4	111	1	116	229	62	2	64	293
52	1030	3380	54	0	4	25	1	39	123	2	81	0	83	206	60	0	60	266
51	1075	3530	108	1	4	94	1	73	281	6	115	0	121	402	56	1	57	459
49	1194	3920	58	0	7	23	2	25	115	3	73	2	78	193	38	1	39	232
48	1249	4100	85	3	9	45	3	49	194	3	185	1	189	383	38	2	40	423
47	1286	4220	72	1	10	38	4	62	187	3	110	0	113	300	41	0	41	341
46	1371	4500	143	0	9	54	3	100	309	4	55	0	59	368	32	0	32	400
45	1432	4700	80	3	12	19	1	44	159	3	51	1	55	214	81	0	81	295
44	1456	4780	68	0	5	21	0	46	140	1	113	2	116	256	28	2	30	286
42	1706	5600	86	2	28	39	3	64	222	4	67	0	71	293	40	6	46	339
41	1770	5810	75	4	6	63	3	73	224	2	110	3	115	339	23	0	23	362
40	1792	5880	0	2	2	2	3	7	16	0	25	1	26	42	231	10	241	283
39	1862	6110	91	8	4	58	14	78	253	9	150	3	162	415	30	2	32	447
38	1889	6200	80	7	10	55	1	96	249	6	162	3	171	420	18	1	19	439
37	1981	6500	41	6	4	18	5	40	114	2	98	1	101	215	32	2	34	249
36	2133	7000	96	5	11	46	2	62	222	6	103	3	112	334	24	0	24	358
35	2194	7200	82	9	6	75	5	110	287	3	75	1	79	366	17	3	20	386
34	2255	7400	51	5	9	37	2	47	151	2	116	1	119	270	11	2	13	283
32	2438	8000	22	1	0	1	6	158	188	2	7	2	11	199	1	0	1	200
31	2468	8100	23	4	4	15	3	29	78	2	113	2	117	195	6	0	6	201
30	2499	8200	39	4	5	25	3	42	118	2	121	0	123	241	8	7	15	256
29	2560	8400	89	10	6	45	4	88	242	1	285	0	286	528	4	1	5	533
28	2590	8500	76	14	7	36	2	62	197	11	180	0	191	388	29	0	29	417
26	2804	9200	49	8	12	19	3	44	135	5	150	0	155	290	34	4	38	328
25	2919	9580	89	6	15	43	1	63	217	4	113	1	118	335	6	1	7	342
24	2926	9600	62	5	16	54	2	79	218	10	102	0	112	330	2	1	3	333
23	2956	9700	37	2	18	16	4	19	96	6	102	0	108	204	6	2	8	212
21	3035	9960	57	5	15	49	13	69	208	3	70	0	73	281	14	2	16	297
20	3041	9980	85	5	15	28	12	80	225	4	121	0	125	350	20	3	23	373
19	3048	10000	58	3	13	19	14	48	155	7	73	2	82	237	10	6	16	253
18	3066	10060	37	1	9	20	3	40	110	7	200	6	213	323	6	0	6	329
16	3078	10100	62	4	21	24	6	50	167	15	83	3	101	268	22	6	28	296
15	3084	10120	35	3	12	8	4	32	94	2	41	2	45	139	7	2	9	148
14	3090	10140	49	2	22	21	3	39	136	1	103	1	105	241	26	5	31	272
13	3096	10160	72	2	19	18	4	43	158	5	100	2	107	265	38	3	41	306
12	3102	10180	64	3	33	39	0	59	198	8	108	2	118	316	25	3	28	344
11	3200	10500	75	4	19	11	2	34	145	5	61	2	68	213	59	3	62	275
10	3297	10820	50	1	8	7	5	30	101	5	40	3	48	149	36	1	37	186
9	3340	10960	72	4	9	5	1	36	127	5	77	3	85	212	42	5	47	259
7	3432	11260	33	5	13	4	4	36	95	4	79	2	85	180	56	6	62	242
5	3541	11620	22	6	13	15	4	40	100	5	55	2	62	162	12	2	14	176
4	3572	11720	35	9	15	11	3	33	106	4	38	2	44	150	51	10	61	211
3	3675	12060	19	2	17	11	0	13	62	1	179	1	181	243	21	8	29	272
2	3779	12400	7	0	2	1	4	8	22	4	170	1	175	197	50	9	59	256
1	3797	12460	23	3	14	3	4	19	66	6	195	1	202	268	99	8	107	375